

Prolyl hydroxylase-dependent proteolysis enables the orthogonal hypoxia responses in plants

Received: 22 June 2025

Accepted: 20 March 2026

Cite this article as: Shukla, V., Iacopino, S., Carbonare, L.D. *et al.* Prolyl hydroxylase-dependent proteolysis enables the orthogonal hypoxia responses in plants. *Nat Commun* (2026). <https://doi.org/10.1038/s41467-026-71366-3>

Vinay Shukla, Sergio Iacopino, Laura Dalle Carbonare, Alessia Del Chiaro, Yuming He, Mauricio Nicolàs Tronca, Thomas P. Keeley, Antonis Papachristodoulou, Beatrice Giuntoli & Francesco Licausi

We are providing an unedited version of this manuscript to give early access to its findings. Before final publication, the manuscript will undergo further editing. Please note there may be errors present which affect the content, and all legal disclaimers apply.

If this paper is publishing under a Transparent Peer Review model then Peer Review reports will publish with the final article.

Title: Prolyl hydroxylase-dependent proteolysis enables the orthogonal hypoxia responses in plants

Authors: Vinay Shukla^{1†}, Sergio Iacopino^{1,2†}, Laura Dalle Carbonare¹, Alessia Del Chiaro¹, Yuming He¹, Mauricio Nicolàs Tronca¹, Thomas P. Keeley^{3,4,5}, Antonis Papachristodoulou⁶, Beatrice Giuntoli^{2*}, Francesco Licausi^{1*}

Affiliations: ¹ Department of Biology, University of Oxford, South Parks Road, OX13RB Oxford, United Kingdom.

² Department of Biology, University of Pisa, Via Luca Ghini 13, 56126, Pisa, Italy.

³ Department of Physiology, Anatomy and Genetics, University of Oxford, OX1 3PT Oxford, United Kingdom.

⁴ Target Discovery Institute, Nuffield Department of Medicine, University of Oxford, Oxford, United Kingdom.

⁵ Ludwig Institute for Cancer Research, Nuffield Department of Medicine, University of Oxford, Oxford, United Kingdom.

⁶ Department of Engineering Science, University of Oxford, Parks Road, Oxford OX13PJ, United Kingdom.

[†]these authors contributed equally

*corresponding authors: beatrice.giuntoli@unipi.it, francesco.licausi@biology.ox.ac.uk

Abstract:

Vascular plants and metazoans use selective proteolysis to control responses to hypoxia, although through distinct biochemical mechanisms. The reason for this divergence is puzzling, since the molecular components necessary for both strategies are conserved. To explore the alternative scenario where plants and animals respond to hypoxia through the same mechanisms, we engineer a three-components system aimed to target proteins for degradation in an oxygen dependent manner *in Arabidopsis thaliana*. When used to control transcription, the synthetic system partially restores hypoxia responsiveness in oxygen-insensitive mutants. Additionally, we demonstrate its potential to regulate growth under flood-induced hypoxia. Our work highlights the use of synthetic biology to reprogram signalling pathways, providing insights into the evolution of oxygen sensing and offering tools for crop improvement under stress conditions.

Introduction

Aerobic organisms require molecular oxygen (O₂) for sufficient ATP synthesis to support growth and development. When O₂ provision to cells from the surrounding environment is limited (hypoxia), cells adjust their structure, physiology and metabolism to avoid or resist the stress. Such adaptations require transcriptional reprogramming triggered by dedicated hypoxia sensing mechanisms. Remarkably, vascular plants and metazoans share a similar sensing strategy based on oxygen-dependent degradation of constitutively expressed transcription factors (TFs) and their nuclear accumulation upon exposure to hypoxia¹. However, this is achieved by different biochemical solutions in the two kingdoms.

In vascular plants, a major role in transcriptional reprogramming is played by the Ethylene Response Factor VII (ERFVII), TFs controlled via the Plant Cysteine Oxidase (PCO)-branch of the N-degron pathway²⁻⁴. This

is a proteasomal degradation pathway that dictates protein stability depending on the exposed N-terminal amino acid⁵. Methionine amino peptidases prepare the ERFVIs to expose an N-terminal cysteinyl residue for N-terminal sulfinylation via PCOs⁶. This modification promotes N-terminal arginylation, which is in turn recognised by the ubiquitin E3 ligase PROTEOLYSIS6 (PRT6), with the assistance of BIG, for polyubiquitination and the consequent degradation through the proteasome⁷⁻⁹ (**Supplementary Fig. 1a**).

Although mammalian cells have an oxygen sensing system based on N-cys oxidation, they regulate transcriptional reprogramming with a different mechanism, relying on the Hypoxia-Inducible Factors (HIFs)^{10,11}. They are dimers of α and β subunits, the former controlled via oxygen-dependent degradation^{12,13}. This regulation is mediated by the hydroxylation of internal prolyl residues, catalysed by O₂ and 2-oxoglutarate (2-OG)-dependent Prolyl-hydroxylases (PHDs)^{14,15}. The hydroxylated HIF α subunit is recognised by a ubiquitin E3 ligase complex through the von Hippel Lindau factor (VHL)^{16,17}. As in the case of the ERFVIs, polyubiquitinated HIF α is degraded by the proteasome. When O₂ levels drop, instead, HIF α is protected from proteolysis and thereby accumulates in the nucleus. Here, heterodimerization with its cognate β -subunit reconstitutes a functional transcription complex able to induce expression of hypoxic genes (**Supplementary Fig. 1b**).

The evident similarity between O₂ sensing strategies from vascular plants and metazoans has led to the speculation that selective proteolysis represents the best solution to accommodate organised multicellularity¹⁸. However, the last common ancestor of plants and animals likely expressed both PHD and N-Cys dioxygenase^{18,19}. This raises the question as to whether PHD adoption better suits O₂ sensing in heterotrophs with an active system for gas circulation, whereas N-Cys dioxygenases optimally accommodate photosynthetic organisms. The recruitment of oxygenases with distinct kinetic parameters as O₂ sensors could reflect substantial differences in the responses produced in the two kingdoms under hypoxia, in the O₂ levels at which these need to be activated and the existence of peculiar mechanisms of interference or crosstalk with metabolites and secondary messengers²⁰⁻²².

Hypotheses regarding the origin and differentiation of molecular mechanisms are traditionally addressed by comparisons across extant species. We reasoned that a synthetic biology approach would instead tackle more directly the question about the convergence/divergence of O₂ sensing mechanisms in animals and plants²³. Therefore, we set out to reconstruct in plant cells a hypoxia-responsive mechanism based on proline hydroxylation and subsequent proteolysis. Previously, we exploited the O₂-dependent interaction of HIF and VHL to engineer a molecular circuit useful to inhibit gene expression in response to hypoxic inputs²⁴. Here, we re-engineered O₂-dependent proteolysis to control the stability of reporters and signal transducers. Besides addressing the fundamental question regarding the evolution and diversification of O₂ sensing in multicellular eukaryotes, we considered that such an effort would serve as a proof of concept for the engineering of proteostatic signalling in plant cells²⁵. Moreover, by doing so, we thought to establish an orthogonal switch to control the response to environmental conditions that limits O₂ availability for plants, such as submergence.

Flooding is one the main causes for agricultural losses worldwide²⁶. Since gas diffusion is severely reduced in water, submerged plant organs experience limited O₂ availability. Tampering with the endogenous O₂ sensing system is likely to compromise plant fitness overall. This is because the N-cys degron pathway controls the response to different environmental stresses including cold, high salinity, pathogen attack and dehydration²⁷⁻²⁹ and also participates to developmental processes³⁰⁻³³. We therefore applied the synthetic biology framework to generate an orthogonal switch for transcriptional regulation in response to hypoxia

in plant cells. We used this molecular device to explore the alternative evolutive scenario where O₂ sensing in plants depends on PHDs and tested its ability to drive developmental responses to submergence-induced hypoxia.

Results

Engineering PHD-dependent proteolysis in plants

We set out to reconstruct an orthogonal O₂-dependent switch for plant cells by inducing targeted proteolysis based on the mammalian HIF-1 α /VHL system (**Supplementary Fig. 1B**). Using the model species *Arabidopsis thaliana*, we have shown previously that the C-terminal Oxygen-dependent degron of HIF-1 α (HIF_{ODD}) and VHL β -domain (aa 63-157) interact in an O₂-dependent manner, exclusively when a human PHD3 enzyme is expressed²⁴. Given the 1.7-1.4 billion years evolutionary distance between plants and animals³⁴, we considered unlikely that the mammalian VHL protein retained the ability to associate with functional E3 ligase complexes in Arabidopsis cells. An initial comparison of *in silico* reconstructed Cullin-Ring E3 ligase (CRLs) complexes from animals and plants suggested similar subunit arrangements between the complex responsible for HIF- α hydroxylation in human cells and those dedicated to auxin signalling in Arabidopsis (**Fig. 1A**). However, while VHL contacts the CRL complex via the interaction between its α -domain with ElonginB (ELOB) and ELOC³⁵ (**Fig. 1A**), the auxin sensor Transport Inhibitor Response1 (TIR1) does so by binding to the Arabidopsis homolog of the mammalian S-phase kinase associated protein 1 (Skp1), Ask1³⁶ (**Fig. 1A**). The α -domain of VHL resembles TIR1 F-box, with a similarly oriented three-helical structure. Nonetheless, VHL's inability to contact Ask1 in Arabidopsis cells is suggested by the distinct amino acid residues involved in VHL/ELOC and F-box/Ask1 interaction, coupled with other minor structural differences (**Supplementary Figure 2A,B**), and by the absence of a Cullin2 homolog in plants³⁷. Therefore, we decided to replace the original α -domain of VHL with an endogenous F-box domain, to enable the incorporation of the chimeric VHL in a CRL E3 ligase complex. Under aerobic conditions, and with the expression of a human PHD3 enzyme²⁴, the chimeric F-box protein would be expected to bind a hydroxylated HIF_{ODD} peptide, thereby promoting the ubiquitination and degradation of the fusion protein in which it is contained. Hypoxia, instead, should prevent recognition and thus stabilise the HIF_{ODD}-tagged protein (**Fig. 1B**).

We first attempted to generate the desired chimeric F-box protein by fusing the F-box domain of TIR1 to VHL β -domain. To monitor HIF degradation, we produced a chimeric transcription factor consisting of the HIF_{ODD} peptide, the minimal GAL4 DNA binding domain and the small but potent activation domain of the Arabidopsis transcription factor Related to APETALA2.12 (RAP2.12)³⁸ (**Fig. 1C**). This construct was expected to bind the synthetic 4xUAS promoter²⁴ and to promote the transcription of a Firefly Luciferase (FLuc) reporter gene (**Fig. 1C**). When expressed in Arabidopsis protoplasts, HIF_{ODD}-GAL4-AD indeed induced FLuc reporter activity, but this was not significantly affected by the presence of VHL-F-box and PHD3 (**Supplementary Fig. 3A,B**). This result suggested the inability of the TIR1-based chimeric VHL to contact the HIF_{ODD} peptide, independently from its hydroxylation state. Therefore, we tested a second F-box domain from the SLEEPY1 (SLY1) protein, one of the smallest functional F-box proteins in the Arabidopsis proteome³⁹, which participates in gibberellin (GA) signalling⁴⁰. Two gibberellin-insensitive SLY1 variants, SLY1-2 and SLY1-10, have been characterised as early protein truncations that abolish gibberellin responsiveness while maintaining intact the F-box domain⁴⁰ (**Supplementary Fig. 4A**). Since no crystal structure for SLY1 is available, we superimposed the predicted model of its F-box domain on TIR1 to verify the conserved identity and position of residues necessary for the interaction with Ask1 (**Supplementary**

Fig. 4B). We fused the wild type and truncated SLY1 variants at the N-terminal end of VHL β -domain and tested them in protoplast, as described before for TIR1. This time, combination of SLY1-VHL with PHD3 abolished FLuc induction by HIF_{ODD}- GAL4-AD, indicating the efficacy of the three chimeric F-box versions at ubiquitinating the hydroxylated transcription factor (**Fig. 1D**). We selected the smallest variant, SLY1-2-VHL, for further experiments, after validating its nuclear localisation (**Supplementary Fig. 4C**), under the assumption that it would interfere the least with GA signalling. Hypoxia alleviated the repression imposed by SLY1-2-VHL on transcription factor activity (**Fig. 1E**), indicating that HIF_{ODD}-GAL4-AD degradation was inhibited when insufficient O₂ availability limited PHD3 activity. This hypothesis was corroborated by immunodetection of GAL4-AD in a western blot (**Fig. 1F**).

PHD-dependent conditional proteolysis is transferable to different reporter proteins

The newly established O₂-dependent proteolytic mechanism could be used to control the stability of other proteins to generate novel types of genetically encoded reporters of hypoxia in plants. To implement this application, we generated single transcriptional units coding for two luciferases (hereafter Luc1 and Luc2, based on their position in the construct) separated by a ubiquitin unit so that, during mRNA translation, deubiquitinases (DUBs) would release two fragments, as described by Bachmair et al.⁴¹. The Luc1-UBQ fragment is suitable for signal normalization whereas the stability of the HIF_{ODD}-fused Luc2 depends on O₂ and PHD3 (**Supplementary Fig. 5A**). We prepared several variants of this construct, distinguished by the combination of three features: the 5' untranslated mRNA region (UTR), the paired luciferases and the number of HIF_{ODD} motifs associated with Luc2. We generated two independent transgenic lines of Arabidopsis stably expressing the SLY1-2-VHL effector along with each reporter variant. Mesophyll protoplasts isolated from each line were then transformed with a *35S:PHD3* construct for testing, or a *35S:GFP* control construct (**Supplementary Fig. 5B**). The desired reporter behaviour consisted in a decreased normoxic output upon PHD3 expression and high output recovery under hypoxia. As the best performing reporter of our set, we thereby identified a construct, driven by the *35S CaMV* promoter, consisting of the *Renilla reniformis* luciferase (RLuc) as Luc1 and of FLuc as Luc2, equipped with a single C-terminal HIF_{ODD} domain (**Fig. 2A,B**). We named this O₂-dependent ratiometric construct as O₂ratio. The other variants showed little responsiveness to either PHD3 or hypoxia, resulting in insufficient dynamic range (**Supplementary Fig. 5C**). To further expand the dynamic range of O₂ratio, we attempted a rational strategy of PHD mutagenesis aimed at lowering its enzymatic activity under low oxygen. Inspired by past studies on the human PHD2 enzyme⁴²⁻⁴⁴, we tested three different single amino-acid substitutions in the transient protoplast system (**Supplementary Fig. 6A,B**). Nevertheless, the wild type PHD3 showed the best performance and had a consistent behaviour across the two independent SLY1-2-VHL/O₂ratio lines used in the analysis (**Supplementary Fig. 6C,D**). We then proceeded to stable transformation the *35S:PHD3* construct in one of them and isolated two independent PHD3 lines (**Supplementary Fig. 6E,F**). Neither of the them showed developmental or growth differences in comparison with wild type plants, indicating substantial orthogonality of the system (**Fig. 2C**). Looking at O₂ratio dynamics in *PHD3*-expressing plants under normoxia and hypoxia, we found that the earliest significant output increase occurred after 6 h hypoxia (**Fig. 2D**).

Finally, we tested the portability of the regulation by transferring the HIF_{ODD} degron to a nuclear VENUS reporter, expressed under the control of the p16 promoter (**Fig. 2E**)⁴⁵. Using confocal microscopy, we could detect a strong fluorescent signal in the root tip of transgenic plants expressing this construct, which

disappeared almost completely after expression of a *PHD3* transgene (**Fig. 2F**). This latter transgenic line recovered nuclear fluorescence when plants were incubated for 6 h at 1% O₂ (**Fig. 2F**). We concluded that the combination of three modules of human origin (*PHD3*, *SLY1-2-VHL* and *HIF_{ODD}*) is a broadly transferable system to control the stability of reporter proteins in plants depending on O₂-availability.

N-cys oxidation and Pro hydroxylation are interchangeable to control hypoxia-dependent protein stability in plant and animal cells

The possibility to establish O₂-dependent, targeted proteolysis allowed us to test an evolutionary scenario where hypoxia signalling did not diverge between vascular plants and metazoans. We did so by wiring the ERFVII transcription factor RAP2.12 to PHD-mediated degradation in Arabidopsis. To this end, we uncoupled RAP2.12 from the PCO-branch of the Arg/N-degron pathway by substituting its N-cys-degron (aa 2-13) with the HIF_{ODD} peptide (**Fig. 3A**). This construct, controlled by the endogenous *RAP2.12* promoter, was expressed together with the *PHD3* and *SLY1-2-VHL* modules in a pentuple *erfVII* mutant³⁰. We applied the same strategy used for O₂ratio to generate independent lines expressing HIF_{ODD}- Δ RAP2.12 and *SLY1-2-VHL* and super-transformed them with a *35S:PHD3* construct (**Supplementary Fig. 7A**). In this case, we used the promoter of the Arabidopsis gene *PCO4*⁴⁶ to control *PHD3*, to ensure similar expression levels of the O₂ sensing modules in the native plant mechanism and the synthetic system. HIF_{ODD}- Δ RAP2.12 stimulated the constitutive activation of the hypoxia marker genes *PCO1* and *SAD6*; co-expression of *PHD3* reversed this phenotype in normoxia but was counteracted by hypoxia (**Supplementary Fig. 7B**). Altogether, this indicated that the synthetic gene circuit is effective in controlling ERFVII activity. We set out to compare the performance of the endogenous and synthetic oxygen sensing systems. Because the *Arabidopsis thaliana* genome codes for five ERFVII⁴⁷, we transformed the *erfVII* mutant with a full RAP2.12 coding sequence, driven by its endogenous promoter, to generate a control genotype with a single ERFVII. We tested the stability of the two RAP2.12 versions in a hypoxia time course by western blot, taking advantage of a fused double human influenza hemagglutinin (2xHA) tag. Wild type RAP2.12 was barely detectable under normoxic conditions and transiently stabilised after 1-2 h hypoxia (**Fig. 3B**, **Supplementary Fig. 8A**). The HIF_{ODD} version of RAP2.12 was more abundant than the native version under normoxia and further increased under hypoxia, although with variable dynamics across repetitions of the experiment (**Fig. 3C**, **Supplementary Fig. 8B,C**). Remarkably, its stability and also reproducibly increased when plants were kept in the dark for 4 h under aerobic conditions (**Supplementary Fig. 8B,C**). As additional validation, we verified that the instability of HIF_{ODD}-RAP2.12 is mediated by PHD3 through the proteasome. Loss of the *PHD3* transgene enhanced HIF_{ODD}-RAP2.12 levels, which were further increased upon treatment of seedlings with the proteasome inhibitor bortezomib (BZ, 50 μ M) (**Fig. 3D**).

These observations suggest a higher efficiency of the N-degron pathway in keeping ERFVII levels low under normoxia when compared with the newly engineered *SLY1.2-VHL* pathway. This could be explained as a refinement evolved over 450 million years, the time estimated for the recruitment of ERFVII⁴⁸ as N-Cys-degron substrates for O₂ sensing⁴⁸. To test this hypothesis, we compared the efficiency of the two O₂-dependent proteolytic systems also in mammalian cells. We employed an immortalized human kidney proximal tubular cell line (HKC-8) previously edited with CRISPR to inactivate the endogenous HIF1 α and HIF2 α ⁴⁹ (**Supplementary Fig. 9A,B**). Opposite to the wild type, these double knock-out (DKO) cells are unable to induce genes that carry a Hypoxia Responsive Element (HRE) in their promoter when exposed to hypoxia⁴⁹. Mirroring our approach with the Arabidopsis RAP2.12, we aimed to obtain a version of HIF-

1 α that is no longer a substrate of PHDs but regulated in an O₂-dependent manner via the N-degron pathway (**Fig. 3E**). We produced three HIF-1 α variants: a wild-type version, one carrying a double substitution on the two proline residues (HIF1 α PPAA) that are hydroxylated by the PHD enzymes (P402A, P564A)⁵⁰ and a third version where HIF1 α PPAA was equipped with the N-cys degron from the human Regulator of G-protein-signalling 4 (RGS4)¹¹ (**Fig. 3E**). We transfected the DKO cells with these constructs and evaluated HIF-1 α protein expression under normoxia and hypoxia. The anti-HIF1 α antibody used for immunoblotting generated a faint band in hypoxic untransformed cells, which likely corresponds to the truncated version produced by CRISPR (**Fig. 3F, Supplementary Fig 9C**). As expected, wildtype HIF-1 α was stabilised under hypoxia whereas the PPAA version was already stable in normoxia (**Fig. 3F, Supplementary Fig 9C**). Remarkably, addition of the RGS4₁₋₁₁ N-degron successfully restored HIF-1 α PPAA O₂-dependent regulation (**Fig. 3F, Supplementary Fig 9C**). We also used a dual luciferase reporter assay based on a synthetic 6xHRE promoter^{51,52} to test how O₂-dependent control of HIF-1 α protein abundance affect transcriptional regulation. Co-transfection of the luciferase reporter together with the empty vector control produced a minimal signal, in line with the lack of functional HIF-1 α in DKO cells⁴⁹ (**Supplementary Fig. 9D**). In contrast, the presence of HIF-1 α resulted in a strong increase of the signal, in an O₂-dependent manner for the wild-type, whereas the PPAA mutant activates the reporter to a comparable extent in normoxic and hypoxic conditions (**Fig. 3G**). Remarkably, the synthetic N-cys-degron version of HIF-1 α had comparable range of induction of the 6xHRE promoter to the wild-type, even though normoxic and hypoxic values were lower (**Figure 3G**). Together with the protein abundance data (**Fig. 3F**), this observation confirmed that the N-degron pathway is more effective at repressing protein accumulation when compared with the VHL pathway, similar to what we observed in plant cells (**Fig. 3B-D**). Overall, we concluded that the N-degron pathway could be a valid alternative to PHD/VHL to adjust HIF-1 α levels in response to the O₂ availability.

PHD-dependent proteolysis can control transcriptional responses to hypoxia in plant cells

Having demonstrated that the PHD-dependent version of RAP2.12 is O₂-regulated in Arabidopsis, we moved on to compare the downstream transcription in response to hypoxia, between the synthetic PHD/VHL-based and the native N-degron pathway-based O₂ sensing. The expression patterns of Hypoxia Responsive Genes (HRG) were first modelled by means of dynamic, ordinary differential equations (ODE). We incorporated in the equations both Michaelis-Menten Kinetics and Mass Action laws to describe the gene expression and biochemical reaction network processes (**Supplementary Fig. S10A,B**). The two models predicted early HRG activation upon exposure to 1% O₂ in both the native and synthetic context, with overall higher expression when ERFVIIIs are controlled by the PHD/VHL degradation pathway (**Fig. 4A**). When HRG expression was simulated as a function of oxygen availability, both systems exhibited nonlinear oxygen-dependent behaviour. However, the response profiles differed markedly: HRG expression increased more gradually across oxygen levels in the PHD/VHL-based system, whereas the PCO-regulated system showed a steeper, more switch-like response (**Fig. 4B**).

We therefore tested these predictions by comparing the induction of hypoxia marker genes in the same *erfVII* complemented plants described in **Fig. 3B,C**. At 1% O₂, the mutant *erfVII* background showed little residual capacity to elicit the expression of *PCO1* and *SAD6* (**Fig. 4C** and **Supplementary Fig. 11A**), as previously reported⁵³. Both complementation strategies caused instead stronger expression of the reporter genes, with time-resolved induction dynamics similar to those predicted by our models (**Fig. 4C, Supplementary Fig. 11A**). We further compared the two O₂-sensing systems in an experimental setup where plants were exposed to a range of sub-atmospheric O₂ concentrations for 2 h. We observed that, while hypoxic gene expression was induced below 10% O₂ in the native N-degron context, in the PHD/VHL context the response appeared only at 1% O₂ (**Fig. 4D** and **Supplementary Fig. 11B**). We expanded this analysis by looking at the entire set of 49 core HRGs⁵⁴ under hypoxia (1% O₂) and near-anoxia (0.1% O₂) in the HIFODD-RAP2.12 line using RNA-seq (**Fig. 4E, Supplementary Data 1**). Overall, the transgenic construct elevated HRG expression, which was severely reduced in the *erfVII* background⁵⁵. Despite the constitutively higher expression in normoxia, 55% of the core HRGs were significantly induced more than 2 fold in the HIFODD-RAP2.12 line while 30% showed a more modest, but still significant upregulation in hypoxia (**Fig. 4E, Supplementary Data 2**). We concluded that ERFVIIIs retain the capacity to activate most HRGs under hypoxia when placed under the control of the PHD/VHL pathway, although with an attenuated dynamic range.

Finally, we compared the tolerance to the hypoxic stress of plants equipped with the two alternative O₂-sensing systems. We subjected 1-week old plants to 1% O₂ for 7 days, under photoperiodic conditions. Both O₂-sensing strategies were associated with decreased lethality as compared to the *erfVII* mutant, although the PCO-regulated RAP2.12 conferred higher fitness than the PHD-regulated version (**Fig. 4F,G, Supplementary Fig. 12A,B**). However, as previously reported³³, higher RAP2.12 abundance in the latter genotype impaired primary root growth, both under aerobic and hypoxic conditions (**Fig. 4H**).

Exploiting PHD-dependent proteolysis to engineer adaptive responses to flooding in plants

Once established that a PDH/VHL-based mechanism for hypoxia sensing can successfully drive transcriptional responses in plant cells, we explored whether the same can be connected to responses that increase plant fitness under O₂ limitation. Reduced O₂ availability commonly occurs because of soil waterlogging or whole plant submergence²⁶. Flood-adapted species have evolved two contrasting strategies: those frequently experiencing long-term and shallow submergence enhance stem and/or petiole elongation to reach the water surface and thus maintain gas exchange ('escape'); those instead exposed to deep or short-lasting floods rather suppress organ elongation and metabolism ('quiescence')⁵⁶. We attempted to promote either response through the synthetic PHD-dependent oxygen sensing. The Arabidopsis ecotype Col-0 exhibits modest organ elongation underwater⁵⁷. To enhance its escape syndrome, we decided to modulate the abundance of the transcription factor Phytochrome Interacting 4 (PIF4), the key regulator of petiole and hypocotyl elongation under shading and warm temperature^{58,59}. We generated a hypoxia-stabilised version of PIF4 fused to the HIF_{ODD} peptide. To minimise interference from other signalling pathways, we selectively mutated specific PIF4 residues whose phosphorylation in response to light, temperature and hormones is known to stimulate proteasomal degradation⁶⁰ (**Fig. 5A**). Therefore, we expected this chimeric PIF4 version to be specifically controlled by hypoxia, due to HIF_{ODD}-dependent proteolysis. We sequentially transformed Col-0 plants with two different T-DNAs, one carrying both the *SLY1-2-VHL* and *pUBQ:HIF_{ODD}-PIF4* cassettes, and a second to express *PHD3*, according to the strategy adopted before (**Supplementary Fig. 5B and 7A**). *HIF_{ODD}-PIF4* over-expression with a *UBQ10* promoter caused an elongated petiole phenotype that could not be inhibited by *PHD3*, despite the use of a strong *35S* promoter (**Supplementary Fig. 13**). We therefore resorted to a moderately active ubiquitous promoter, from the *ROTUNDA3* (*RON3*, *At4g24500*) gene, to control the *HIF_{ODD}-PIF4* transgene. We selected two independent lines for which we could segregate *PHD3* out (**Supplementary Fig. 14A**) and confirmed that hypoxia (1% O₂, 6 h) was able to increase HIF_{ODD}-PIF4 protein but not mRNA (**Fig. 5B,C** and **Supplementary Fig. 14B,C**). These plants exhibited slower leaf production and accelerated flowering (**Supplementary Fig. 14D,E**). The latter phenotype could result from increased PIF4 activity, reported to promote reproductive transition in Arabidopsis⁶¹, in the chronically hypoxic shoot apical meristem⁶². Expression of *pRON3:PIF4-HIF_{ODD}* significantly stimulated growth of both hypocotyl and petiole length, a phenotype that was reversed, at least in part, by co-expression of *PHD3* (**Supplementary Fig. 14F-H**). This indicated that our strategy to adopt PHD/VHL-dependent degradation of developmental regulators is successful at controlling organ elongation. Finally, we tested whether environmental hypoxia could relieve the repression imposed by *PHD3* and *SLY1-2-VHL* on the chimeric *HIF_{ODD}-PIF4* (**Fig. 5D**). We submerged 15-days-old plants with distilled water and measured petiole growth after 4 days (**Fig. 5E,F**). The wild type exhibited moderate elongation, which was insufficient to push the leaves near the water surface (**Fig. 5E**). Under the same water column, petioles of the transgenic plants grew twice as much, bringing blades closer to the atmosphere (**Fig. 5E,F**). This result confirmed the possibility to adopt the PDH/VHL-based hypoxia sensing system to control growth in response to changes in ambient O₂ availability.

Discussion

With this work, we engineered an orthogonal hypoxia responsive system for plant cells inspired by the O₂-dependent degradation of the mammalian HIF proteins (**Fig. 1B**). We showed that this system is applicable to control stability, and thus activity, of different proteins, resulting in the possibility to modulate different outputs in an O₂ sensing system. This approach aligns with those aimed to orthogonally control protein stability in mammalian and plant cells⁶³⁻⁶⁵. Successful engineering of selective proteolysis has been achieved with proteolysis- and autophagy-targeting chimeras^{66,67}, strategies that hold great potential for

therapeutic applications and more recently explored also for agricultural applications⁶⁸. Our exercise diverges from these in its aim to connect the output to a stimulus, cell O₂ concentration, which is affected by both endogenous and external factors.

The process of design, test and optimization of the components required for this molecular device to perform the desired function highlighted old, and revealed new, opportunities and limitations of applying the synthetic biology framework to complex multicellular organisms. First, we confirmed that single cell systems, such as transiently transformed protoplasts, can be effectively used to test the performances of genetic circuits (**Fig. 1C-F and 2A-C**), before successful export to stable transformation in whole plants (**Fig. 3-5**). For example, our system performed similarly in both contexts, when it was used to control the stability of luciferase reporters (**Supplementary Fig. 2B and Fig. 2D**). Differences in output dynamic range seemed to be associated with the kind of protein used as reporter, as highlighted in our applications of the system to generate low O₂ reporters based on luminescence or fluorescence (**Fig. 2B,D and F**).

One of the main challenges faced in this exercise of biological engineering was the difficulty to estimate, and account for, the heterogeneous behavior of each component in a multicellular system. For example, cis-acting regulatory elements, such as promoters and regulatory mRNA untranslated regions, are strongly affected by their context, such as the chromatin state, which can differ greatly between cell types. As one of the few attempts to implement multi-components genetic circuits in plants⁶⁹⁻⁷¹, it was interesting to observe the strong effect that alternative elements produced on the output (**Supplementary Fig. 5C**). This consideration becomes even more relevant when the genetic circuit relies on the control of protein stability, a process for which the characterization of components is more limited than transcription and translation. Such a limitation highlights the need of the community to produce quantitative characterisation of degradation determinants. Despite these constraints, the success of our strategy paves the way for further optimisation and implementation. Our attempts to alter output dynamics using structure-inspired PHD mutations that impact the catalytic site and neighboring residues did not succeed (**Supplementary Fig. 6D-E**), highlighting the difficulties in increasing the sensitivity of dioxygenases to hypoxia while maintaining high activity under aerobic conditions. The PHDs' gas tunnel is a promising alternative target to test in the future, based on the enhanced hydroxylation efficiency achieved in mammalian cells⁷².

Swapping of O₂ sensing mechanisms between animal and plant cells (**Fig. 3**) is an exercise that interfaces with both fundamental and applied research. From a fundamental perspective, it allows experimental testing of the evolution of O₂ sensing in eukaryotes and its diversification between plants and animals. Intriguingly, both kingdoms adopted proteostatic control of transcription factors, on top of which additional regulatory mechanisms exist, to reprogram cells to cope with reduced oxygen availability. While it has been speculated that this is a requirement and the optimal solution for the multicellular organization that involves stem cells¹⁸, it is puzzling that animals and plants diverged so much when their last common ancestor likely contained the biochemical functions to perform both N-cys-degron and VHL-dependent degradation. Successful control of transcriptional responses rewiring endogenous transcriptional regulators to PHD-primed degradation in *Arabidopsis* allows us to exclude intrinsic metabolic or signaling interference that would prevent this mechanism from working.

Animal cells control responses to hypoxia via the Cys branch of the N-degron pathway¹¹, although none of the N-Cys degron substrates characterized so far are transcription factors. This enables regulation of cellular processes occurring outside the nucleus, such as at the plasma membrane, in the cytoplasm, and

in other cellular compartments⁷³⁻⁷⁵. It is tempting to speculate that this pathway also provides a faster response system to fluctuating O₂ levels than the HIF-based pathway, as it directly modulates the activity of regulatory proteins rather than requiring transcription and translation to elicit a response. In contrast, evidence for the involvement of PHD activity in regulating protein stability in plant cells is lacking, although less direct roles for these enzymes in plant responses to hypoxia have been proposed⁷⁶.

Differences in the regulation of transcriptional responses to hypoxia in plant and animal cells may also derive from the distinct ways in which cells in these organisms experience oxygen limitation. While chronic hypoxia of specific cell types, including stem cells, is characteristic of both systems^{77,78}, acute hypoxia is typically more deleterious in metabolically active animals, where ischemia and subsequent reoxygenation cause rapid cellular damage^{79,80}. In many metazoans, oxygen delivery through circulatory systems helps meet tissue oxygen requirements. Plants, by contrast, lack active oxygen transport and are generally more resilient to hypoxia, particularly during short-term exposure⁸¹. Moreover, plant cells are more likely to experience hyperoxia as a result of photosynthetic oxygen production^{82,83}. The combination of these metabolic and anatomical constraints has likely played a major role in shaping the architecture of oxygen-sensing systems in the two kingdoms.

This study also revealed the existence of additional regulation exerted on RAP2.12, which determines the transiency of its accumulation in hypoxia, and its increase in the dark (**Figure 3B-C, Supplementary Fig. 8A-B**). Similar, although slower, dynamics have been reported for the ERFVII RAP2.3³⁰. Remarkably, target gene expression correlated with the protein abundance of native and synthetic RAP2.12 at early timepoints in the comparison between aerobic and hypoxic plants. This was not observed at later time points, which is likely explained by additional post-translational modifications, including phosphorylation that controls RAP2.12's nuclear localization and transactivation capacity^{84,85}. N-degron dependent control of HIF stability, upstream of PHD regulation, has been proposed recently⁸⁶. While it has been shown that N-cysteine oxidation determines substrate stability with similar O₂-sensitivity to prolyl-hydroxylation in animal cells⁸⁷, our swap exercise of O₂ sensing system between plant and animal cells hinted at higher proteolytic efficacy for the N-degron pathway when compared with VHL-promoted degradation. It is tempting to speculate that this might reflect the need to switch on adaptive responses at different O₂ levels.

In summary, we successfully generated a PHD- and O₂-dependent degradation of selected proteins through the engineering of a chimeric F-box protein. The evolutionary question of why animals and plants rely on different dioxygenases to control the stability of transcription factors that regulate hypoxia-responsive gene expression remains far from fully answered. Nevertheless, our results show that these systems are, in fact, functionally interchangeable across kingdoms, providing a foundation for future efforts in rational design or directed evolution aimed at matching gene expression dynamics to those governed by endogenous pathways.

By adding the HIF_{ODD} fragment to different reporters and effector modules, we demonstrated the possibility to monitor cell oxidic states as well as to drive advantageous developmental traits for submergence tolerance. From an applied perspective, wiring the synthetic O₂ sensing system to control petiole elongation in *Arabidopsis* (**Fig. 5**) pioneers, together with other studies⁸⁸, the engineering of adaptive responses to environmental cues. While it remains to be established whether promotion of fast petiole elongation can be useful in specific agroecosystems, it is possible to connect the novel O₂ sensing mechanism to repressors of petiole elongation, thus favoring the quiescent syndrome typical of flash

flood-tolerant species. The highly transgenic nature of the system prevents its immediate application in agriculture in many countries; nevertheless, it demonstrates feasibility and potential for synthetic biology to improve crops' ability to cope with abiotic stresses, including those exacerbated by climate change. While we here conveniently used *Arabidopsis* as a testbed, given the compatibility of molecular components and the availability of simple transformation and selection protocols, the chimeric O₂ sensing system is likely exportable to many other crops, including monocots.

ARTICLE IN PRESS

Methods

Plant materials and growth conditions

The *Arabidopsis thaliana* Columbia-0 (Col-0) ecotype was used as the wild-type background in all the experiments. The *erfVII* mutant³⁰, which carries T-DNA insertions in the genes *At1g72360*, *At2g47520*, *At1g53910*, *At3g14230* and *At3g16770*, was provided by Michael J. Holdsworth. Plants were either grown in soil on a peat:perlite 3:1 mixture, or in sterility on agarized (8 g l⁻¹) half-strength Murashige and Skoog (MS) medium supplemented with 1% sucrose, after sterilization with 70% ethanol and 10% commercial bleach solution and 5 washes with sterile distilled water. In both cases, seeds were vernalized at 4°C for 48 h in the dark and then germinated at 22°C day/18°C night with a photoperiod of 12 h. The plant material was subjected to short-duration low-oxygen treatments as specified in the text and figure legends by flushing a mixture of pure nitrogen (N₂) and compressed air to reach the desired O₂ concentration inside hermetic boxes. For treatments longer than 24 h, we instead used a Hypoxic Workstations (Whitley). For submergence treatments, plants grown in sterility in magenta boxes were submerged with water at an approximate depth of 3 cm. The treatment began at the end of the day for a period of 72 hours.

Generation of transgenic plants

A. thaliana plants were transformed with *Agrobacterium tumefaciens* applying the floral-dip method⁸⁹. Selection of transformed plants was carried out using appropriate antibiotics or herbicides or fluorescent seed selection. Transgene presence was assessed by PCR.

In silico protein complex assembly

The structure of the Cul1-Rbx1-Ask1-TIR1 complex was predicted based on atomic coordinates from the Protein Data Bank (PDB) entries 2P1Q and 2P1O (10.1038/nature05731) which include the TIR1 and ASK1 protein structures, and AlphaFold⁹⁰ entries AF-Q94AH6-F1-v4 and AF-Q940X7-F1-v4, representing the Arabidopsis Cullin1 and Rbx1 structures, respectively.

Similarly, the Cul1-Rbx1-Ask1-SLY1 complex structure was predicted using the PDB entry 2P1Q containing the Ask1 protein structure, alongside AlphaFold entries AF-Q94AH6-F1-v4, AF-Q940X7-F1-v4 and AF-Q9STX3-F1-v4 which correspond to Cul1, Rbx1 and SLY1, respectively. AlphaFold models AF-Q94AH6-F1-v4, AF-Q940X7-F1-v4 and AF-Q9STX3-F1-v4 were retrieved from the AlphaFold protein structure database. Structural predictions of the Cul1-Rbx1-Ask1 complex with TIR1 and SLY1 were carried out using the full Cul1-Rbx1-Skp1-Skp2 complex as template (PDB: 1LDJ⁹¹).

The structure of the SCF complex Cul2-Rbx1-EloB-EloC-VHL-HIF_{ODD} was predicted using atomic coordinates 1LQB⁹² and 1VCB⁹⁰, which include ELOB, ELOC, VHL and HIF_{ODD}, and 5N4W⁹³, which provides the structure for VHL, ELOB, ELOC, Cul2 and Rbx1. Structural alignment and figure rendering were performed using VMD and PyMol software.

DNA cloning and assembly

Transcriptional units were either cloned from genomic DNA, cDNA or *de novo* synthesized by GeneArt (Thermo-Fisher Scientific). Protein-coding sequences were codon optimized using the EMBOSS Backtranseq online tools⁹⁴. A full list of synthetic sequences and plasmids used in this work is provided in **Supplementary Table 1** and **2**, respectively. All maps of the plasmids used in this work are provided as **Supplementary Data 3**. DNA fragments provided of a 5'-CACC additional sequence or flanked by restriction sites were initially sub-cloned either in the pENTR/D-TOPO[®] vector, to be recombined into

destination vectors using Gateway™ LR Clonase™ II Enzyme mix (catalog number 11791020, Thermo-Fisher Scientific), or in the pCR™2.1-TOPO®-TA vector (Thermo-Fisher Scientific), to be inserted into expression vectors via a restriction-ligation strategy, respectively. Plasmid maps were generated with Serial Cloner (Serial basic).

For protoplast transformation, the 35S:FboxTIR1-VHL, 35S:HIF_{ODD}-GAL4DBD-RAP2.12AD-3xFLAG, 35S:SLY1-VHL, 35S:SLY1-2-VHL and 35S:FboxSLY1-10-VHL plasmids were generated from synthetic coding sequences, purchased as DNA strings from GeneArt (Thermo-Fisher Scientific), further ligated in the pENTR/D-TOPO® vector (Thermo-Fisher Scientific) and recombined into the p2GW7⁹⁵ vector via Gateway™ cloning. The 4xUAS:Fluc plasmid has been described in Bui et al. (2015)³⁸. The 35S:PHD3 plasmid has been described in Iacopino et al. (2019)²⁴

The O₂ratio construct was produced by overlapping PCR. A 5'-terminal 3xHA-Renilla-UBQ fragment was amplified with the primers 3xHA-Fw and UBQ-Rv using the C-DLOR plasmid⁹⁶ as template, while the fragment bearing the Firefly Luciferase CDS fused to the HIF_{ODD} was amplified with the primers UBQ_Luc-Fw and Luc_HIF_Rv using the 4XUAS:Fluc plasmid³⁸ as a template. The Luc_HIF_Rv primer was designed to include the full HIF_{ODD} coding sequence. The two fragments were joined together with a second PCR using the oligonucleotides 3xHA-Fw and Luc_HIF_Rv. The resulting PCR product was cloned into the pENTR/D-TOPO®. The construct 35S:O₂Ratio/pUBQ:SLY1,2-VHL used for Arabidopsis infiltration was generated in three steps. First, a synthetic construct consisting of the Arabidopsis UBQ10 promoter⁹⁷, flanked by the SacI and AfeI restriction sites, and followed by the 35S CaMV terminator⁹⁸, flanked by EcoRI and a further SacI restriction site, was ligated into the pK7WG2⁹⁵ plasmid using the compatible SacI restriction site. Then, the SLY1-2 coding sequence was cloned in between the UBQ10 promoter and 35S CaM terminator using the AfeI and EcoRI restriction sites, to obtain a destination plasmid named pK7WG2/pUBQ10:SLY1-2. Finally, this destination was recombined with the entry plasmid containing O₂ratio via Gateway™ cloning.

The NLS-O₂ratio and O₂ratio² variants were generated by restriction/ligation cloning operated on the O₂ratio entry vector. SacI and XbaI were used to remove a portion of the UBQ10 and FLuc sequence, and a DNA fragment designed to contain the excised regions and the additional HIF_{ODD} or NLS element was ligated using same restriction sites. The nanO₂ratio² entry vector was synthesized by GeneArt (Thermo Fisher Scientific). The nanO₂ratio variants were generated by digesting the nanO₂ratio² entry vector using the SacI and XhoI restriction sites and ligating an identical DNA sequence devoid of the first HIF-COOD. To replace the CaMV 35S Omega leader with the 5'UTR region of the Arabidopsis *ADH1* gene, pK7WG2/pUBQ10:SLY1-2 was cut with StuI and SpeI and ligated with a synthetic DNA string containing the excised region of the 35S promoter followed by *ADH1* 5'-UTR, flanked by compatible restriction sites thereby turning the original vector into the new pK7WG35SUTR^{ADH}/pUBQ10: SLY1-2 Gateway destination vector.

All O₂ratio variants entry vector were then recombined using Gateway™ cloning in these two destination vectors to generate the binary expression vectors reported in **Supplementary Figure 5**.

The NLS-VENUS-HIF_{ODD} construct was purchased as DNA string from Geneart (Thermo-Fisher Scientific) and ligated into the pENTR/D-TOPO®. The p16:NLS-VENUS-HIF_{ODD}/pUBQ: SLY1-2-VHL plasmid was generated by recombination of the NLS-VENUS-HIF_{ODD} entry with pK7WG2/pUBQ10:SLY1-2 and subsequent replacement of the 35S promoter. Specifically, the expression plasmid was cut with StuI and SacI restriction enzymes and ligated with a compatible p16 promoter sequence⁴⁵ amplified using primers p16_Fw and p16_Rv and from a p16-FLIPnls43 template vector⁹⁹.

The construct pRAP2.12:HIF_{ODD}-2xHA-D13RAP2.12/pUBQ:SLY1-2-VHL was generated as follows: a synthetic DNA string containing the chimeric HIF_{ODD}-2xHA-D13RAP2.12 coding sequence was ligated in pENTR/D-TOPO® and recombined with the pK7WGpUBQ10:SLY1-2 destination vector. A 2kb-long upstream region of the *RAP2.12* promoter was amplified using NcoI_pRAP_Fw and NcoI_pRAP_Rv from Arabidopsis genomic DNA. The 35S promoter was then removed from the expression plasmid using NcoI

restriction enzyme and substituted with the *RAP2.12* promoter fragment via ligation. Finally, the kanamycin plant selection marker was removed using *Apal* and *Cpol* restriction enzymes, to be replaced with a fluorescent selection cassette. The *pOLE_Fw* and *mCHERRY_Rv* primers were used with a *pKIR1.0*¹⁰⁰ template plasmid, to amplify an expression cassette consisting of the Arabidopsis oleosin promoter (*pOLE1*) and a downstream fusion sequence between the red fluorescent protein *mKATE2* and the oleosin gene (*OLE1*). This fluorescent cassette, flanked by compatible *Apal* and *Cpol* sites, was subsequently ligated with the backbone obtained before. The construct *pRAP2.12:RAP2.12-2xHA* was synthesized in an entry plasmid by GeneArt (Thermo-Fisher Scientific) and subsequently recombined into the *pH7WG*⁹⁵ binary vector via Gateway™ cloning.

To generate the *pPCO4:PHD3* expression vector, the *PHD3* entry plasmid was recombined Gateway™ cloning in the plasmid *pH7WG-promPCO4*⁴⁶. The expression plasmid was digested with *Apal* and *Cpol* and an expression cassette consisting of the Arabidopsis *At2S3* promoter driving GFP expression amplified from *pFP91*¹⁰¹ with primers *At2S3_Fw* and *t35S_Rv* and subsequently ligated. *PHD3* mutations were obtained by site directed mutagenesis with *PHD3Asp137His Fw* and *Rv*, *PHD3Asp137Glu Fw* and *Rv* and *PHD3Arg205Lys Fw* and *Rv*. The *HIF_{ODD}-PIF4* sequence were purchased as DNA string and ligated into the *pENTR/D-TOPO*®. The *pSIC:PIF4-HIF_{ODD}/pUBQ:SLY1-2-VHL* plasmid was obtained by recombining the *PIF4-HIS* entry into the *pK7WG2/pUBQ:SLY1-2* and replacing the 35S *CaMV* promoter using *Stul* and *SpeI* restriction site. The *SIC/RON3* promoter was amplified by PCR using primers *pAt4g24500_Fw* and *pAt4g24500_Rv* using *Col-0* genomic DNA as template and then ligated using compatible restriction sites.

Hypoxia, submergence, and bortezomib treatments

For hypoxia treatments, 7-day-old in vitro-grown seedlings were exposed to hypoxia (specified in each figure legend as % O_2/N_2 [v/v]) for 6 h in the dark (starting at 8 a.m.), while control plants were kept in the dark under atmospheric conditions (21% O_2). For Western blot or qRT-PCR analyses, each biological replicate consisted of at least five seedlings. For submergence tolerance assays, 14-day-old seedlings grown in Magenta boxes were submerged in 60 mL of distilled water for 4 d in the dark. Control plants were kept in the dark without submergence. Bortezomib (CAS 179324-69-7; Santa Cruz Biotechnology) treatments were conducted on 7-day-old Arabidopsis seedlings transferred to six-well plates containing fresh half-strength MS medium supplemented with 50 μ M BZ or 0.02% DMSO (mock control) for 3 h.

Protoplasts transformation and transactivation assay

Protoplasts isolation and transformation were performed as reported by Yoo et al.,¹⁰² with the modifications described in Iacopino et al.²⁴. Firefly and Renilla luciferase activity was measured using the Dual-Luciferase® Reporter Assay System (E1910, Promega), Nanoluciferase and Firefly luciferase activity was measured using Nano-Glo® Dual-Luciferase® Reporter Assay System (N1610, Promega). Relative luciferase activity for O_2 ratio variants was calculated as the ratio between the *HIF_{ODD}-linked* luciferase and the *HIF_{ODD}-independent* luciferase.

Phenotypic analyses

Petiole and hypocotyl lengths were measured from images using ImageJ software¹⁰³. Petioles were pressed between two layers of Scotch tape and scanned with an EPSON Perfection V750 PRO scanner at a 400 DPI resolution. Hypocotyl images were captured using a Nikon Coolpix P520 digital camera. Root lengths were measured from images scanned from plastic square plates using ImageJ software.

Human cell culture and hypoxia exposure

HKC-8 wild type and DKO cells were cultured in Dulbecco's Modified Eagle Medium, supplemented with 10% fetal bovine serum, 2mM L-Glutamine, 100 U/ml penicillin and 10 µg/ml streptomycin. Cells were maintained at 37 °C under an atmosphere of 5% CO₂ in air. Hypoxic incubations were conducted in an atmosphere-regulated workstation set at 1% O₂: 5% CO₂: balance N₂ (Invivo 400, Baker-Ruskin Technologies).

Genomic DNA extraction from DKO cells

Genomic DNA was extracted from cell pellets by incubation in lysis buffer (100mM Tris pH 8.0, 5mM EDTA, 200 mM NaCl, 0.2% SDS and 100 µg/ml Proteinase K) with 18 shaking at 55 °C for 2 h, followed by isopropanol precipitation and 70% ethanol wash. Precipitated genomic DNA was re-suspended in water. Genomic target regions were PCR amplified with gHIF1/2α primers mentioned in **Supplementary Table 1** using the PrimeSTAR® GXL DNA Polymerase according to the manufacturer's protocol using 30 cycles, 98 °C denaturation temperature and 60 °C annealing temperature. PCR products were separated using agarose gel electrophoresis. DNA was then purified with QIAquick® PCR Purification Kit (Qiagen) and Sanger sequenced.

Luciferase assays from human cell cultures

Luciferase assays were conducted using the Dual Luciferase Reporter kit (Promega) and measurements taken using the Fluostar® Omega Microplate Reader. In experiments that did not include RnLuc expression, the step involving the Stop & Glo Reagent was omitted. Human cells grown in 12-well plates were co-transfected with 500 ng of PGL3 PGK6 TkPluc and 100 ng of PGL4 RL plasmid DNA⁵². 6-8 h after transfection, cells were incubated in normoxia (21% O₂) or hypoxia (1% O₂) for 16-18 h. After the incubation period, cells were washed in phosphate buffered saline, lysed with 100 µl 1X Passive lysis buffer and incubated at -80 °C for at least 2h. Homogenised Arabidopsis tissues and protoplasts were similarly lysed with 100 µl 1X Passive lysis buffer. Prior to measurement, cell lysates were spun at max speed at room temperature for 2 min using a benchtop centrifuge. Firefly luciferase activity was assayed by combining 6 µl cell lysate with 30 µl Luciferase Assay Reagent II (or 10 µl cell lysate + 50 µl LAR II). Renilla luciferase was measured by adding of an equal volume of the Stop & Glo Reagent.

Generation of stable cell lines

HKC-8 DKO cells were transfected with pcDNA3 plasmid carrying HIF1 α -, HIF1 α PPAA, RGS41-11-HIF1α PPAA using GeneJuice® (Novagen). After 24 h, cells were seeded at limiting dilution in selective medium containing 0.8 mg/ml G418. Resistant clones were isolated and expanded. Clones stably expressing HIF1α proteins, were identified by transfection with PGL3 PGK6 TkPluc and PGL4 RL vectors and luciferase assay, as described above, to detect HIF1α transcriptional activity.

Confocal imaging

Confocal investigations were performed using a Zeiss LSM800 confocal microscope. For sub-cellular localization studies, GFP fluorescence was excited with 488 nm laser light and collected with a 497-554 nm long-pass emission filter. Chlorophyll autofluorescence was excited at 633 nm and collected at 650–750 nm. Nuclei were stained with 1µg µl⁻¹ 4',6-diamidino-2-phenylidone (DAPI, Sigma-Aldrich), and fluorescence excited at 405 nm and collected at 410-470 nm. For Venus visualization in roots, plants were stained with 10 µg µl⁻¹ propidium iodide (PI) (Sigma-Aldrich) cell wall stain. The roots were observed with 20x objective lens under ZEISS LSM 800 Laser Confocal Scanning Microscope. HIF-NLS-Venus seedlings were fixed with 4% paraformaldehyde and stained with ClearSee¹⁰⁴ supplemented with 1 µl/ml SCRI

Renaissance 2200 (SR2200). Venus fluorescence was excited with 488 nm laser light and collected with a 520-560 nm. PI was excited with 488 nm laser light and collected at 650-700 nm. Images were analyzed with the ZEN 2010 software (Zeiss).

SDS-PAGE and immunoblotting

Total Arabidopsis proteins were isolated from 1-week old seedlings grown on vertical plates using a buffer containing 50mM Tris (pH7.5), 0.1% w/v SDS and Protease Inhibitor Cocktail (cOmplete™, Mini, EDTA-free Protease Inhibitor Cocktail, Sigma-Aldrich; 11836170001). From leaf mesophyll protoplasts, total proteins were instead extracted using a buffer containing Laemmli and 5% v/v β-mercaptoethanol. Equal total protein amount (70 μg) were resolved by SDS-PAGE and then transferred to PVDF membrane using MiniTrans-Blot electrophoretic transfer cell (Bio-Rad). To detect the HA tag, membranes were probed with anti-HA primary antibody (Sigma-Aldrich; H3663) at 1:2,000 dilution. Membranes were then probed with HRP-conjugated anti-mouse secondary antibody (Sigma-Aldrich; 12-349) at 1:10,000 dilution. To detect the FLAG-tagged GAL4 activation domain, membranes were probed with the monoclonal HRP-conjugated, anti-FLAG antibody (A8592, Sigma-Aldrich) at 1:1,000 dilution. Immunoblots were developed with SuperSignal™ West Pico PLUS Chemiluminescent Substrate (Thermo Fisher Scientific) using the iBright CL1500 Imaging System (Thermo Fisher Scientific). To detect HIF_{ODD}-PIF4, a recombinant anti PIF4 antibody was used (AS163955, 2B Scientific) at 1:1000 dilution. Membranes were then probed with HRP-conjugated anti-goat secondary antibody (AS09 605, Agrisera) at 1:10,000 dilution.

For immunoblot analyses of human cells, ~1 x 10⁶ cells were washed in phosphate buffered saline, lysed in SDS lysis buffer (50 mM Tris pH 6.8, 2% SDS, 10% Glycerol), sonicated, and mixed with Laemmli 6X SDS-PAGE sample buffer. Proteins were then separated using a 9% SDS-PAGE gel, transferred to polyvinylidene difluoride membrane (Immobilon-P, Millipore) and blocked in 4% fat free milk (in phosphate-buffered saline containing 0.1% Tween 20). Primary antibodies used were: Purified Mouse Anti-Human HIF-1α (610959, BD Transduction Laboratories™) and anti-HIF-2α (mouse monoclonal, 190b). HRP-conjugated secondary antibodies (DAKO) and chemiluminescence substrate (West Dura, 34076, Thermo Fisher Scientific) were used to visualize proteins, using the ChemiDOc XRS+ imaging system (BioRad). After immunoblot imaging, membranes were stained with Coomassie brilliant blue to visualise total protein, as a reference for sample loading.

Plant RNA isolation and qPCR analyses

Total RNA was extracted from 100 mg of frozen-ground seedlings as described previously³³. One microgram of total RNA was treated with DNase (Thermo Scientific™) to remove genomic DNA before retro-transcription using qPCRBIO cDNA Synthesis Kit (PCR Biosystems). Real-time quantitative PCRs were performed in 10 μl volume using a 2X Power SYBR™ Master Mix (Thermo Fisher Scientific™), 10 ng cDNA and 0.2 μM of specific reverse and complement primers for each gene to be tested. Thermal cycling and fluorescence acquisition was carried out with StepOnePlus™ Real-Time PCR System. Ubiquitin10 (*AT4G0532*) was used as housekeeping genes for Arabidopsis analysis. A full list of the primers used for qPCR is included in **Supplementary Table 1**. Relative expression of each individual gene was calculated using the 2^{-ΔΔCt} method¹⁰⁵.

RNA sequencing

RNA was isolated using GeneJET RNA Purification Kit (Thermo Scientific™) as per manufacturer's instruction. Genomic DNA and cDNA library preparation were carried out as described in Dalle Carbonare et al.⁴⁸. Libraries were sequenced on an Illumina NovaSeq 6000 platform. Reads cleaning, mapping and counting was performed as described in Dalle Carbonare et al.⁴⁸ and differential expression analysis was

performed using the DESeq2 R package (v1.20.0), with p values adjusted by the Benjamini-Hochberg method to control for FDR.

Statistical analysis

Ordinary two-way and one-way analysis of variance (ANOVA) and multiple comparisons for statistical differences were performed with R or GraphPad Prism 9 for Windows 10.

Mathematical modelling of RAP2.12/PCO4 and HIF-RAP2.12/PHD kinetics

Model description and assumptions. The two models that were developed to describe the expression dynamics of Hypoxia Responsive Genes (HRG) in either the PHD/VHL- or the N-degron pathway-based oxygen sensing system consist of two coupled Ordinary Differential Equations (ODEs). Within these equations, we incorporated both Michaelis-Menten Kinetics and Mass Action laws to describe the gene expression and biochemical reaction network processes (**Supplementary Tables 3 and 4**)¹⁰⁶. The overall processes involving RAP2.12 expression, degradation, and downstream HRGs activation were illustrated in **Supplementary Fig. S10A**.

In our models, the RAP2.12 protein is synthesized at a rate k_1 and degraded at a rate k_2 . In the *promRAP2.12:RAP2.12-2xHA* scenario, where RAP2.12 is the only ERFVII expressed in plant cells, the N-Cys-degron pathway promotes O₂-dependent RAP2.12 degradation following Michaelis-Menten kinetics, with catalytic constant k_3 , and Michaelis constants K_{m1} and K_{m2} . In this system, HRGs expression, which in our model is assumed to be exclusively driven by RAP2.12, follows Michaelis-Menten kinetics at a rate represented by k_4 and K_{m3} and decay occurring at a rate of k_5 . In the HIF_{ODD}-RAP2.12 system, we applied the same parameters for RAP2.12 protein synthesis and degradation as well as for HRG activation. However, in this chimeric system, HIF_{ODD}-RAP2.12 undergoes O₂-dependent degradation through enzymatic prolyl-hydroxylation, characterized by rates k_6 , K_{m4} , and K_{m5} . Since the production and degradation rates of RAP2.12 are unknown, we used the HIF α protein production and degradation rates from the literature. Similarly, the PHD concentration was set to 0.1 μ M based on published models¹⁰⁷. These assumptions do not affect the validity of our conclusions.

To simplify our model, we assume that all reactions occur in a homogeneous environment, without accounting for compartmentalization or specific microenvironments within the cell. We further assume that each reaction species—such as RAP2.12, PCO, PHD, O₂, and mRNA—is evenly distributed throughout the system. To focus on the oxidation and hydroxylation processes, we simplify the model by assuming that RAP2.12 and HIF_{ODD}-RAP2.12 are degraded instantly following N-Cys and Pro oxidation, respectively. Additionally, for comparability, we assume identical concentrations of PCO and PHD and at steady state under normoxic conditions that characterise the initial timepoint in the simulation. These enzyme concentrations are assumed to remain constant after exposure to 1% hypoxia. In a short timeframe, this is not unrealistic since protein synthesis is strongly reduced under hypoxia¹⁰⁸. By maintaining the same levels of PCO and PHD, we can compare the dynamic hypoxic responses based solely on their catalytic activities. Accordingly, the model was designed as a constrained, hypothesis-generating framework that emphasized relative system behaviour under standardized conditions rather than absolute quantitative prediction across experimental platforms.

Non-linear fitting and simulation. We used MATLAB's 'Welsh' and 'Fair' weight functions within the `nlinfit` function. The rate constants k_3 , K_{m1} , and K_{m2} were re-fitted for the PCO-mediated degradation of RAP2.12, while k_6 , K_{m4} , and K_{m5} were re-fitted for the PHD-mediated degradation of HIF_{ODD}-RAP2.12. This three-dimensional nonlinear fitting, which is depicted in **Supplementary Fig. S10B**, was performed based on published kinetic data^{22,109}. All parameters are listed in **Supplementary Table 5**.

To simulate hypoxic responses, the initial concentrations of RAP2.12/HIF_{ODD}-RAP2.12 and mRNA as inputs were obtained from steady-state simulations conducted under normoxic conditions (21% O₂) for 6 h (**Supplementary Table 4**). Subsequently, dynamic simulations of hypoxic responses (**Fig. 4A**) were conducted under 1% O₂ conditions for 4 h. Steady-state oxygen–response curves (**Fig. 4B**) were generated by simulating the model at a range of fixed oxygen concentrations (0.1–21%). For each oxygen level, the system was integrated for 6 h to reach steady state, and the simulated HRG expression was recorded.

Data Availability

Raw RNA sequencing data from this study are available in the Gene Expression Omnibus (GEO) under accession number [GSE315308](https://www.ncbi.nlm.nih.gov/geo/query/acc.cgi?acc=GSE315308). Uncropped western blot images are available in Zenodo (10.5281/zenodo.18074079). All additional data supporting the findings of this study that are not included in the article, Supplementary Information or Source Data are available from the corresponding authors upon request for non-commercial academic research; requests will be evaluated within 4 weeks and, if approved, data will be shared via a secure file-transfer link. Source data are provided with this paper.

Code availability: The equations used to generate the results reported in this study are available in the materials and methods and supplementary information sections. The code is available at the link: <https://github.com/ymiplant/orthogonal-hypoxia-responses-plants.git>

References

1. Holdsworth, M. J. & Gibbs, D. J. Comparative Biology of Oxygen Sensing in Plants and Animals. *Current Biology* **30**, R362–R369 (2020).
2. Gibbs, D. J. *et al.* Homeostatic response to hypoxia is regulated by the N-end rule pathway in plants. *Nature* **2011 479:7373 479**, 415–418 (2011).
3. Licausi, F. *et al.* Oxygen sensing in plants is mediated by an N-end rule pathway for protein destabilization. *Nature* **2011 479:7373 479**, 419–422 (2011).
4. Weits, D. a *et al.* Plant cysteine oxidases control the oxygen-dependent branch of the N-end-rule pathway. *Nat. Commun.* **5**, 3425 (2014).
5. Varshavsky, A. N-degron and C-degron pathways of protein degradation. *Proceedings of the National Academy of Sciences of the United States of America* vol. 116 Preprint at <https://doi.org/10.1073/pnas.1816596116> (2019).
6. White, M. D. *et al.* Plant cysteine oxidases are dioxygenases that directly enable arginyl transferase-catalysed arginylation of N-end rule targets. *Nat. Commun.* **8**, 1–9 (2017).
7. Graciet, E. *et al.* The N-end rule pathway controls multiple functions during Arabidopsis shoot and leaf development. *Proceedings of the National Academy of Sciences* **106**, 13618–13623 (2009).
8. Garzón, M. *et al.* PRT6/At5g02310 encodes an Arabidopsis ubiquitin ligase of the N-end rule pathway with arginine specificity and is not the CER3 locus. *FEBS Lett.* **581**, 3189–3196 (2007).
9. Zhang, H. *et al.* BIG enhances Arg/N-degron pathway-mediated protein degradation to regulate Arabidopsis hypoxia responses and suberin deposition. *Plant Cell* **36**, 3177–3200 (2024).
10. Semenza, G. L., Nejfelt, M. K., Chi, S. M. & Antonarakis, S. E. Hypoxia-inducible nuclear factors bind to an enhancer element located 3' to the human erythropoietin gene. *Proc. Natl. Acad. Sci. U. S. A.* **88**, (1991).
11. Masson, N. *et al.* Conserved N-terminal cysteine dioxygenases transduce responses to hypoxia in animals and plants. *Science* **365**, 65–69 (2019).
12. Maxwell, P. H. *et al.* The tumour suppressor protein VHL targets hypoxia-inducible factors for oxygen-dependent proteolysis. *Nature* **399**, (1999).
13. Jiang, B. H., Rue, E., Wang, G. L., Roe, R. & Semenza, G. L. Dimerization, DNA binding, and transactivation properties of hypoxia- inducible factor 1. *Journal of Biological Chemistry* **271**, (1996).
14. Bruick, R. K. & McKnight, S. L. A conserved family of prolyl-4-hydroxylases that modify HIF. *Science* (1979). **294**, (2001).
15. Jaakkola, P. *et al.* Targeting of HIF- α to the von Hippel-Lindau ubiquitylation complex by O₂-regulated prolyl hydroxylation. *Science* (1979). **292**, (2001).
16. Iliopoulos, O., Kibel, A., Gray, S. & Kaelin, W. G. Tumour suppression by the human von hippel-lindau gene product. *Nat. Med.* **1**, (1995).

17. Ivan, M. *et al.* HIF α targeted for VHL-mediated destruction by proline hydroxylation: Implications for O₂ sensing. *Science* (1979). **292**, (2001).
18. Hammarlund, E. U., Flashman, E., Mohlin, S. & Licausi, F. Oxygen-sensing mechanisms across eukaryotic kingdoms and their roles in complex multicellularity. *Science* (1979). **370**, (2020).
19. Gorres, K. L. & Raines, R. T. Prolyl 4-hydroxylase. *Critical Reviews in Biochemistry and Molecular Biology* vol. 45 Preprint at <https://doi.org/10.3109/10409231003627991> (2010).
20. Tarhonskaya, H. *et al.* Kinetic investigations of the role of factor inhibiting hypoxia-inducible factor (FIH) as an oxygen sensor. *Journal of Biological Chemistry* **290**, (2015).
21. Ehrismann, D. *et al.* Studies on the activity of the hypoxia-inducible-factor hydroxylases using an oxygen consumption assay. *Biochemical Journal* **401**, (2007).
22. White, M. D., Kamps, J. J. A. G., East, S., Taylor Kearney, L. J. & Flashman, E. The plant cysteine oxidases from *Arabidopsis thaliana* are kinetically tailored to act as oxygen sensors. *Journal of Biological Chemistry* **293**, 11786–11795 (2018).
23. Garner, K. L. Principles of synthetic biology. *Essays in Biochemistry* vol. 65 Preprint at <https://doi.org/10.1042/EBC20200059> (2021).
24. Iacopino, S. *et al.* A synthetic oxygen sensor for plants based on animal hypoxia signaling. *Plant Physiol.* **179**, (2019).
25. Orosa, B. *et al.* Plant proteostasis – shaping the proteome: a research community aiming to understand molecular mechanisms that control protein abundance. in *New Phytologist* vol. 227 (2020).
26. Bailey-Serres, J. & Voesenek, L. A. C. J. Flooding stress: Acclimations and genetic diversity. *Annual Review of Plant Biology* vol. 59 Preprint at <https://doi.org/10.1146/annurev.arplant.59.032607.092752> (2008).
27. Gibbs, D. J. *et al.* Nitric oxide sensing in plants is mediated by proteolytic control of group VII ERF transcription factors. *Mol. Cell* **53**, 369–79 (2014).
28. Akter, S. *et al.* H₂O₂ repurposes the plant oxygen-sensing machinery to control the transcriptional response to oxidative stress. *bioRxiv* 2024.10.21.619351 (2024) doi:10.1101/2024.10.21.619351.
29. Valeri, M. C. *et al.* Botrytis cinerea induces local hypoxia in *Arabidopsis* leaves. *New Phytologist* **229**, (2021).
30. Abbas, M. *et al.* Oxygen sensing coordinates photomorphogenesis to facilitate seedling survival. *Current Biology* **25**, 1483–1488 (2015).
31. Meitha, K. *et al.* Developmental control of hypoxia during bud burst in grapevine. *Plant Cell Environ.* **41**, (2018).
32. Weits, D. A. *et al.* An apical hypoxic niche sets the pace of shoot meristem activity. *Nature* 2019 569:7758 **569**, 714–717 (2019).

33. Shukla, V. *et al.* Endogenous hypoxia in lateral root primordia controls root architecture by antagonizing auxin signaling in Arabidopsis. *Mol. Plant* **12**, 538–551 (2019).
34. Bowles, A. M. C., Williamson, C. J., Williams, T. A. & Donoghue, P. C. J. Cryogenian Origins of Multicellularity in Archaeplastida. *Genome Biol. Evol.* **16**, (2024).
35. Ashouri, K., Mohseni, S., Tourtelot, J., Sharma, P. & Spiess, P. E. Implications of Von Hippel-Lindau Syndrome and Renal Cell Carcinoma. *Journal of Kidney Cancer* **2**, 163–173 (2015).
36. Tan, X. *et al.* Mechanism of auxin perception by the TIR1 ubiquitin ligase. *Nature* **446**, (2007).
37. Choi, C. M., Gray, W. M., Mooney, S. & Hellmann, H. Composition, Roles, and Regulation of Cullin-Based Ubiquitin E3 Ligases. *Arabidopsis Book* **12**, (2014).
38. Bui, L. T., Giuntoli, B., Kosmacz, M., Parlanti, S. & Licausi, F. Constitutively expressed ERF-VII transcription factors redundantly activate the core anaerobic response in Arabidopsis thaliana. *Plant Science* **236**, 37–43 (2015).
39. Kuroda, H. *et al.* Classification and expression analysis of Arabidopsis F-box-containing protein genes. *Plant Cell Physiol.* **43**, (2002).
40. McGinnis, K. M. *et al.* The Arabidopsis SLEEPY1 Gene Encodes a Putative F-Box Subunit of an SCF E3 Ubiquitin Ligase. *Plant Cell* **15**, 1120–1130 (2003).
41. Bachmair, A., Finley, D. & Varshavsky, A. In vivo half-life of a protein is a function of its amino-terminal residue. *Science (1979)*. **234**, 179–186 (1986).
42. Chowdhury, R. *et al.* Structural basis for oxygen degradation domain selectivity of the HIF prolyl hydroxylases. *Nature Communications* 2016 7:1 **7**, 1–10 (2016).
43. Chowdhury, R. *et al.* Structural basis for binding of hypoxia-inducible factor to the oxygen-sensing prolyl hydroxylases. *Structure* **17**, 981–989 (2009).
44. Tarhonskaya, H. *et al.* Investigating the contribution of the active site environment to the slow reaction of hypoxia-inducible factor prolyl hydroxylase domain 2 with oxygen. *Biochemical Journal* **463**, 363–372 (2014).
45. Schuster, C. *et al.* A regulatory framework for shoot stem cell control integrating metabolic, transcriptional, and phytohormone signals. *Dev. Cell* **28**, (2014).
46. White, M. D. *et al.* Structures of Arabidopsis thaliana oxygen-sensing plant cysteine oxidases 4 and 5 enable targeted manipulation of their activity. *Proc. Natl. Acad. Sci. U. S. A.* **117**, (2020).
47. Licausi, F. *et al.* HRE1 and HRE2, two hypoxia-inducible ethylene response factors, affect anaerobic responses in Arabidopsis thaliana. *The Plant Journal* **62**, 302–315 (2010).
48. Dalle Carbonare, L. *et al.* ERFVIIIs as transducers of oxygen-sensing in the evolution of land plant response to hypoxia. *Mol. Plant* **18**, 1072–1087 (2025).
49. Smythies, J. A. *et al.* Inherent DNA -binding specificities of the HIF -1 α and HIF -2 α transcription factors in chromatin . *EMBO Rep.* **20**, (2019).

50. Huang, L. E., Gu, J., Schau, M. & Bunn, H. F. Regulation of hypoxia-inducible factor 1 α is mediated by an O₂-dependent degradation domain via the ubiquitin-proteasome pathway. *Proc. Natl. Acad. Sci. U. S. A.* **95**, 7987–7992 (1998).
51. Firth, J. D., Ebert, B. L., Pugh, C. W. & Ratcliffe, P. J. Oxygen-regulated control elements in the phosphoglycerate kinase 1 and lactate dehydrogenase A genes: Similarities with the erythropoietin 3' enhancer. *Proc. Natl. Acad. Sci. U. S. A.* **91**, 6496–6500 (1994).
52. Doran, D. M., Kulkarni-Datar, K., Cool, D. R. & Brown, T. L. Hypoxia Activates Constitutive Luciferase Reporter Constructs. *Biochimie* **93**, 361 (2010).
53. Carbonare, L. D. *et al.* The role of ERFVIs as oxygen-sensing transducers in the evolution of land plant response to hypoxia. *bioRxiv* 2024.09.27.615240 (2024) doi:10.1101/2024.09.27.615240.
54. Mustrup, A. *et al.* Profiling translomes of discrete cell populations resolves altered cellular priorities during hypoxia in Arabidopsis. *Proc. Natl. Acad. Sci. U. S. A.* **106**, 18843–18848 (2009).
55. Dalle Carbonare, L. *et al.* ERFVIs as transducers of oxygen-sensing in the evolution of land plant response to hypoxia. *Mol. Plant* **18**, 1072–1087 (2025).
56. van Veen, H. *et al.* Two Rumex species from contrasting hydrological niches regulate flooding tolerance through distinct mechanisms. *Plant Cell* **25**, (2013).
57. Vashisht, D. *et al.* Natural variation of submergence tolerance among Arabidopsis thaliana accessions. *New Phytologist* **190**, (2011).
58. Legris, M., Nieto, C., Sellaro, R., Prat, S. & Casal, J. J. Perception and signalling of light and temperature cues in plants. *Plant Journal* **90**, (2017).
59. Zhou, D., Wang, X., Wang, X. & Mao, T. PHYTOCHROME INTERACTING FACTOR 4 regulates microtubule organization to mediate high temperature-induced hypocotyl elongation in Arabidopsis. *Plant Cell* **35**, (2023).
60. Favero, D. S. Mechanisms regulating PIF transcription factor activity at the protein level. *Physiol. Plant.* **169**, (2020).
61. Kumar, S. V. *et al.* Transcription factor PIF4 controls the thermosensory activation of flowering. *Nature* 2012 484:7393 **484**, 242–245 (2012).
62. Weits, D. A. *et al.* An apical hypoxic niche sets the pace of shoot meristem activity. *Nature* 2019 569:7758 **569**, 714–717 (2019).
63. Yesbolatova, A. *et al.* The auxin-inducible degron 2 technology provides sharp degradation control in yeast, mammalian cells, and mice. *Nat. Commun.* **11**, (2020).
64. Caussin, E., Kanca, O. & Affolter, M. Fluorescent fusion protein knockout mediated by anti-GFP nanobody. *Nat. Struct. Mol. Biol.* **19**, (2012).
65. Huang, L. & Rojas-Pierce, M. Rapid depletion of target proteins in plants by an inducible protein degradation system. *Plant Cell* **36**, (2024).

66. Churcher, I. Protac-Induced Protein Degradation in Drug Discovery: Breaking the Rules or Just Making New Ones? *J. Med. Chem.* **61**, (2018).
67. Ji, C. H. *et al.* The AUTOTAC chemical biology platform for targeted protein degradation via the autophagy-lysosome system. *Nat. Commun.* **13**, (2022).
68. Leon, R. G. & Bassham, D. C. PROTAC for agriculture: learning from human medicine to generate new biotechnological weed control solutions. *Pest Manag. Sci.* **80**, (2024).
69. Khan, M. A. *et al.* CRISPRi-based circuits to control gene expression in plants. *Nature Biotechnology* 2024 43:3 **43**, 416–430 (2024).
70. Brophy, J. A. N. *et al.* Synthetic genetic circuits as a means of reprogramming plant roots. *Science* (1979). **377**, 747–751 (2022).
71. Lloyd, J. P. B. *et al.* Synthetic memory circuits for stable cell reprogramming in plants. *Nat. Biotechnol.* **40**, 1862–1872 (2022).
72. Windsor, P. *et al.* Gas Tunnel Engineering of Prolyl Hydroxylase Reprograms Hypoxia Signaling in Cells. *Angewandte Chemie International Edition* e202409234 (2024) doi:10.1002/ANIE.202409234.
73. Heathcote, K. C. *et al.* N-terminal cysteine acetylation and oxidation patterns may define protein stability. *Nature Communications* 2024 15:1 **15**, 5360- (2024).
74. Bekturova, A., Makaros, Y., Ben-David, S. & Koren, I. Global profiling of N-terminal cysteine–dependent degradation mechanisms. *Proc. Natl. Acad. Sci. U. S. A.* **122**, e2501681122 (2025).
75. Kastnes, M. *et al.* The pro-tumorigenic cytokine IL-32 has a high turnover in multiple myeloma cells due to proteolysis regulated by oxygen-sensing cysteine dioxygenase and deubiquitinating enzymes. *Front. Oncol.* **13**, 1197542 (2023).
76. Vlad, F. *et al.* Involvement of arabidopsis prolyl 4 hydroxylases in hypoxia, anoxia and mechanical wounding. *Plant Signal. Behav.* **2**, 368–369 (2007).
77. Suda, T., Takubo, K. & Semenza, G. L. Metabolic Regulation of Hematopoietic Stem Cells in the Hypoxic Niche. *Cell Stem Cell* **9**, 298–310 (2011).
78. Weits, D. A., van Dongen, J. T. & Licausi, F. Molecular oxygen as a signaling component in plant development. *New Phytologist* **229**, 24–35 (2021).
79. Saikumar, P., Dong, Z., Weinberg, J. M. & Venkatachalam, M. A. Mechanisms of cell death in hypoxia/reoxygenation injury. *Oncogene* **17**, 3341–3349 (1998).
80. Li, C. & Jackson, R. M. Reactive species mechanisms of cellular hypoxia-reoxygenation injury. <https://doi.org/10.1152/ajpcell.00112.2001> **282**, (2002).
81. Gibbs, J. & Greenway, H. Review: Mechanisms of anoxia tolerance in plants. I. Growth, survival and anaerobic catabolism. *Functional Plant Biology* **30**, 353–353 (2003).

82. Saikumar, P., Dong, Z., Weinberg, J. M. & Venkatachalam, M. A. Mechanisms of cell death in hypoxia/reoxygenation injury. *Oncogene* **17**, 3341–3349 (1998).
83. Punkkinen, M. *et al.* Mitochondria affect photosynthesis through altered tissue levels of O₂. *Plant Physiol.* **200**, 648 (2026).
84. Fan, B. *et al.* Calcium-dependent activation of CPK12 facilitates its cytoplasm-to-nucleus translocation to potentiate plant hypoxia sensing by phosphorylating ERF-VII transcription factors. *Mol. Plant* **16**, 979–998 (2023).
85. Kunkowska, A. B. *et al.* Target of rapamycin signaling couples energy to oxygen sensing to modulate hypoxic gene expression in Arabidopsis. *Proc. Natl. Acad. Sci. U. S. A.* **120**, e2212474120 (2023).
86. Moorthy, B. T. *et al.* The evolutionarily conserved arginyltransferase 1 mediates a pVHL-independent oxygen-sensing pathway in mammalian cells. *Dev. Cell* **57**, (2022).
87. Tian, Y. M., Holdship, P., To, T. Q., Ratcliffe, P. J. & Keeley, T. P. Comparative analysis of N-terminal cysteine dioxygenation and prolyl-hydroxylation as oxygen-sensing pathways in mammalian cells. *Journal of Biological Chemistry* **299**, (2023).
88. Hayakawa, T., Suzuki, H., Yamamoto, H. & Mitsuda, N. Synthetic biology in plants. *Plant Biotechnology* **41**, 173–193 (2024).
89. Clough, S. J. & Bent, A. F. Floral dip: a simplified method for *Agrobacterium*-mediated transformation of *Arabidopsis thaliana*. *The Plant Journal* **16**, 735–743 (1998).
90. Jumper, J. *et al.* Highly accurate protein structure prediction with AlphaFold. *Nature* **2021** 596:7873 **596**, 583–589 (2021).
91. Zheng, N. *et al.* Structure of the Cul1–Rbx1–Skp1–F boxSkp2 SCF ubiquitin ligase complex. *Nature* **2002** 416:6882 **416**, 703–709 (2002).
92. Hon, W. C. *et al.* Structural basis for the recognition of hydroxyproline in HIF-1 α by pVHL. *Nature* **2002** 417:6892 **417**, 975–978 (2002).
93. Cardote, T. A. F., Gadd, M. S. & Ciulli, A. Crystal Structure of the Cul2-Rbx1-EloBC-VHL Ubiquitin Ligase Complex. *Structure* **25**, 901-911.e3 (2017).
94. Lopez, R., Cowley, A., Li, W. & McWilliam, H. Using EMBL-EBI Services via Web Interface and Programmatically via Web Services. *Curr. Protoc. Bioinformatics* **48**, 3.12.1-3.12.50 (2014).
95. Karimi, M., Inzé, D. & Depicker, A. GATEWAY vectors for *Agrobacterium*-mediated plant transformation. *Trends Plant Sci.* **7**, 193–5 (2002).
96. Puerta, M. L. *et al.* A ratiometric sensor based on plant N-terminal degrons able to report oxygen dynamics in *Saccharomyces cerevisiae*. *J. Mol. Biol.* **431**, 2810–2820 (2019).
97. Grefen, C. *et al.* A ubiquitin-10 promoter-based vector set for fluorescent protein tagging facilitates temporal stability and native protein distribution in transient and stable expression studies. *The Plant Journal* **64**, 355–365 (2010).

98. Hirt, H., Kögl, M., Murbacher, T. & Heberle-Bors, E. Evolutionary conservation of transcriptional machinery between yeast and plants as shown by the efficient expression from the CaMV 35S promoter and 35S terminator. *Curr. Genet.* **17**, (1990).
99. Rizza, A., Walia, A., Lanquar, V., Frommer, W. B. & Jones, A. M. In vivo gibberellin gradients visualized in rapidly elongating tissues. *Nat. Plants* **3**, (2017).
100. Tsutsui, H. & Higashiyama, T. pKAMA-ITACHI Vectors for Highly Efficient CRISPR/Cas9-Mediated Gene Knockout in *Arabidopsis thaliana*. *Plant Cell Physiol.* **58**, 46–56 (2017).
101. Kroj, T., Savino, G., Valon, C., Giraudat, J. & Parcy, F. Regulation of storage protein gene expression in *Arabidopsis*. *Development* **130**, 6065–6073 (2003).
102. Yoo, S.-D., Cho, Y.-H. & Sheen, J. *Arabidopsis* mesophyll protoplasts: a versatile cell system for transient gene expression analysis. *Nat. Protoc.* **2**, 1565–1572 (2007).
103. Rueden, C. T. *et al.* ImageJ2: ImageJ for the next generation of scientific image data. *BMC Bioinformatics* **18**, (2017).
104. Ursache, R., Andersen, T. G., Marhavý, P. & Geldner, N. A protocol for combining fluorescent proteins with histological stains for diverse cell wall components. *Plant Journal* **93**, 399–412 (2018).
105. Livak, K. J. & Schmittgen, T. D. Analysis of Relative Gene Expression Data Using Real-Time Quantitative PCR and the 2- $\Delta\Delta$ CT Method. *Methods* **25**, 402–408 (2001).
106. He, Y. & Papachristodoulou, A. Prolyl hydroxylase-dependent proteolysis enables orthogonal hypoxia responses in plants. <https://doi.org/10.5281/ZENODO.18736224>
doi:10.5281/ZENODO.18736224.
107. Nguyen, L. K. *et al.* A dynamic model of the hypoxia-inducible factor 1a (HIF-1a) network. *J. Cell Sci.* **128**, (2015).
108. Branco-Price, C., Kaiser, K. A., Jang, C. J. H., Larive, C. K. & Bailey-Serres, J. Selective mRNA translation coordinates energetic and metabolic adjustments to cellular oxygen deprivation and reoxygenation in *Arabidopsis thaliana*. *Plant Journal* **56**, (2008).
109. Tarhonskaya, H. *et al.* Investigating the contribution of the active site environment to the slow reaction of hypoxia-inducible factor prolyl hydroxylase domain 2 with oxygen. *Biochemical Journal* **463**, (2014).

Acknowledgments

Funding: European Research Council Grant 101001320 ‘Synoxys’ and Italian Ministry of University and Research PRIN grant 20173EWRT9 (FL); Biotechnology and Biological Sciences Research Council Interdisciplinary Doctoral Programme (BB/T008784/1, YH) and BB/Z516946/1 (FL, VS). Oxford University Press John Fell Fund 0009776 (FL, SI).

Author contributions:

Conceptualization: VS, SI, BG, FL

Methodology: VS, SI, LDC, ADC, YH, TPK, AP, MNT

Investigation: VS, SI, LDC, ADC, YH, TPK

Visualization: SI, VS

Funding acquisition: FL, SI

Project administration: FL, BG

Supervision: FL, BG, AP

Writing – original draft: SI, VS, FL, BG

Writing – review & editing: TPK, AP

Competing interests: Authors declare that they have no competing interests.

Figure 1. Implementation of PHD- and VHL-dependent O₂-sensing in plant cells. **A.** Comparison of the predicted human VBC-CR (left) and plants SCF^{Tir1} (right) complexes. The VBC-CR complex comprises the scaffold protein Cul2 (grey), the E3 ubiquitin ligase Rbx1 (light brown), the adaptor proteins EloB (aquamarine) and EloC (blue) and the substrate recognition protein VHL (α -domain in yellow, β -domain in bronze). The plant SCF complex consists of the Cul1 scaffold protein (grey), Rbx1 (light brown), the adaptor Ask1 (blue) and the substrate recognition F-box protein TIR1 (LRR region in yellow, F-box domain in green). The peptides shown for the animal and plant substrates are HIF_{ODD} and IAA7, respectively. **B.** The O₂-dependent proteolytic mechanism engineered for plant cells. A chimeric E3 ligase, which comprises the VHL beta domain and a plant F-box domain, recognizes the HIF_{ODD} domain when this is hydroxylated by PHD in the presence of O₂. Reporter proteins linked to the HIF_{ODD} are degraded in normoxia but stable in hypoxia. **C.** Reporter strategy deployed to test the synthetic O₂ sensing system. HIF_{ODD} was fused to the DNA binding domain of GAL4 and the activation domain (AD) of RAP2.12. In the presence of O₂, this chimeric transcription factor is degraded by the proteasome. In hypoxic conditions, instead, it is stabilised and binds the 4xUAS promoter, to activate transcription of a FLuc reporter. **D.** FLuc output measured in Arabidopsis mesophyll protoplasts transformed with combinations of plasmids to express HIF_{ODD}-GAL4-AD, three variants of the SLY1-VHL chimera (**Supplementary Fig. 4A**) and PHD3. Letters indicate statistically significant differences ($p \leq 0.05$), as determined by one-way ANOVA followed by Tukey's post-hoc test ($n = 4$ independent biological replicates, each replicate consisting of protoplasts isolated from an independent batch of plants and measured as the average of technical luciferase readings.). Data are shown as box plots, where the centre line indicates the median, box bounds indicate the 25th and 75th percentiles, whiskers extend to the minimum and maximum values, and all points represent individual biological replicates. **E.** Effect of hypoxia (1% O₂, 6 h) on FLuc output in protoplasts expressing HIF_{ODD}-GAL4-AD, SLY1-2-VHL and PHD3. Letters indicate statistically significant differences ($p \leq 0.05$), as determined by two-way ANOVA followed by Tukey's post-hoc test ($n = 4$ independent biological replicates, each replicate consisting of protoplasts isolated from an independent batch of plants and measured as the average of technical luciferase readings.). Data are shown as box plots, where the centre line indicates the median, box bounds indicate the 25th and 75th percentiles, whiskers extend to the minimum and maximum values, and all points represent individual biological replicates. **F.** Immunodetection of HIF_{ODD}-GAL4-AD using a anti FLAG antibody in the same experimental setup as **E.**

Figure 2. Design and testing of a ratiometric PHD- and VHL-dependent O₂ reporter in plants.

A. O₂ratio, a polyprotein consisting of Renilla Luciferase (RLuc), a UBQ10 unit and FLuc-HIF_{ODD}, was expressed in plant cells together with PHD3 and SLY1-2-VHL (not shown). Endogenous ubiquitin proteases (UBPs) co-translationally cleave the polypeptide at the C-terminus of UBQ10. The resulting RLuc serves as a normalization reference while FLuc-HIF_{ODD} is used to monitor O₂ levels. **B.** PHD- and O₂-dependent stability of O₂ratio in protoplasts that express the modules described in A. Letters indicate statistical differences ($p \leq 0.05$) determined by two-way ANOVA followed by Tukey's post-hoc test ($n = 4$ independent biological replicates, each replicate consisting of protoplasts isolated from an independent batch of plants and measured as the average of technical luciferase readings.). Data are shown as box plots, where the centre line indicates the median, box bounds indicate the 25th and 75th percentiles, whiskers extend to the minimum and maximum values, and all points represent individual biological replicates. **C.** Phenotype of 4-week-old O₂ratio and wild-type plants (scale – 1cm). Representative image of 5 observations. **D.** O₂ratio output dynamics in *35S:PHD3* O₂ratio seedlings during a hypoxia (1% O₂, yellow) or normoxia (21% O₂, gray) time course. The relative luminescence output was normalized to the average FLuc/RLuc value at time 0 h. Letters indicate statistical difference ($p \leq 0.05$) between treatments at each time point, as assessed by one-way ANOVA followed by Tukey's post-test ($n=4$). **E.** The fluorescent protein Venus, fused with a nuclear localization signal (NLS) and HIF_{ODD}, serves as a reporter of O₂ levels. **F.** Stability of the Venus fluorescence signal when regulated by PHD activity and atmospheric O₂ availability in root tips of 7-day old Arabidopsis seedlings subjected to 21% or 1% O₂ for 6 h (scale – 50 μm). Representative image of 7 observations.

Figure 3. Complementation of the hypoxia-insensitive *erfVII* mutant by synthetic PHD-based oxygen sensing. **A.** In *A. thaliana*, RAP2.12 stability is regulated in an O₂-dependent manner through the PCO/N-degron pathway (left). A chimeric RAP2.12 is instead controlled by the synthetic PHD/VHL regulatory module. To achieve this, the N-terminal 13 aa were removed from RAP2.12 (Δ RAP2.12), to bypass PCO regulation, and substituted with HIF_{ODD}. Under normoxia, HIF_{ODD}- Δ RAP2.12 is expected to undergo PHD-dependent degradation. **B.** Immunodetection of RAP2.12 and **C.** of HIF_{ODD}- Δ RAP2.12 following a treatment with 1% O₂ for 4 hours. Ponceau staining of total proteins is shown as the loading control. The *erfVII* background (1% O₂, 2 h) is shown as a negative control for both transgenic lines. The experiment was repeated independently 2 times with similar results. **D.** Immunoblot detection of HIF_{ODD}- Δ RAP2.12 in 7-day-old seedlings expressing or not expressing human PHD3, following treatment with 50 μM bortezomib (BZ) or mock (0.02% DMSO). The experiment was repeated independently 2 times with similar results. **E.** In mammalian cells, HIF-1 α stability is regulated in an O₂-dependent manner through the PHD/VHL pathway (left). A chimeric HIF-1 α is instead controlled by the ADO/N-degron pathway (right). To achieve this, Pro402 and Pro564 were substituted with Ala to bypass PHD regulation and the N-cys degron of RGS4 (aa1-11) was added. Under normoxia, RGS4₁₋₁₁-HIF-1 α is expected to undergo ADO-dependent degradation. **F.** Immunodetection of HIF-1 α in DKO cells transiently transfected with plasmids coding for wild type HIF-1 α , HIF-1 α (PPAA) and RGS4₁₋₁₁-HIF-1 α (PPAA) and treated with 21% or 1% O₂ for 16 h. Coomassie blue staining of total proteins is shown as the loading control. The experiment was repeated independently 2 times with similar results. **G.** Fluc/RLuc signal at 21% O₂ and 1% O₂ (16 h) of transiently transfected DKO cells ($n = 4$ independent biological replicates, each replicate corresponding to an independently transfected well of HKC-8 DKO cells measured once for Firefly and Renilla luciferase.). Statistical significance of differences was assessed by unpaired two-tailed t-test (*: $p < 0.05$, **: $p < 0.01$, ***: $p < 0.001$, and ****: $p < 0.0001$). Data are shown as box plots, where the centre line indicates the

median, box bounds indicate the 25th and 75th percentiles, whiskers extend to the minimum and maximum values, and all points represent individual biological replicates.

Figure 4. Functional characterization of native and synthetic O₂ sensing mechanisms. A-B. Predicted induction of a generic hypoxia-responsive gene (HRG) by RAP2.12 under the control of either the PCO oxygen-sensing mechanism or the PHD synthetic sensing pathway. **(A)** HRG expression over a simulated 4-h treatment at 1% (v/v) O₂. **(B)** HRG expression across a range of O₂ concentrations spanning from 21% to 0.1%. **C.** Expression of the HRG *SAD6* in 7-day-old Arabidopsis *erfVII* seedlings and complementation lines expressing RAP2.12-HA (teal) or HIF_{ODD}-ΔRAP2.12-HA (pink) grown under normoxia and then subjected to 21 or 1% O₂ for 0.5 to 4 hours. Statistical significance of hypoxic gene expression relative to 21% O₂ controls is denoted by asterisks (t-test, $p \leq 0.05$). **D.** Dynamics of *SAD6* marker gene expression in response to different O₂ levels in *erfVII* plants expressing RAP2.12-HA under control of the PCO or PHD pathways in an *erfVII* background. Letters indicate statistical significance of hypoxic treatments compared with 21% O₂ within each genotype, analysed independently by one-way ANOVA and followed by Tukey's post-hoc test ($p \leq 0.05$). **E.** Heatmap showing the effect of 2 h of hypoxia (at 1% or 0.1% O₂) in HIF_{ODD}-ΔRAP2.12-HA/*erfVII* plants on Fragments Per Kilobase of transcript per Million mapped reads (FPKM) of core hypoxia-response genes. Data for wild type and *erfVII* are taken from Dalle Carbonare et al.⁵⁵. **F.** Hypoxia tolerance assay of *erfVII* mutants and complemented lines expressing RAP2.12-HA or HIF_{ODD}-ΔRAP2.12-HA. Seven-day-old seedlings were grown on agar plates and exposed to 1% O₂ for seven days, followed by a seven-day recovery period. Images were taken at the end of the recovery period. **G.** Plant tolerance after hypoxia ($n \geq 36$). Inset images illustrate representative status for categorisation and quantification. **H.** Primary root length of seedlings from **(D)** at the end of the 7-day hypoxia treatment. Letters indicate statistical significance, with two-way ANOVA and Tukey's post-test ($p \leq 0.05$, n = number of individual seedlings per genotype and condition and is indicated below each box.). Data are shown as box plots, where the centre line indicates the median, box bounds indicate the 25th and 75th percentiles, whiskers extend to the minimum and maximum values, and all points represent individual biological replicates.

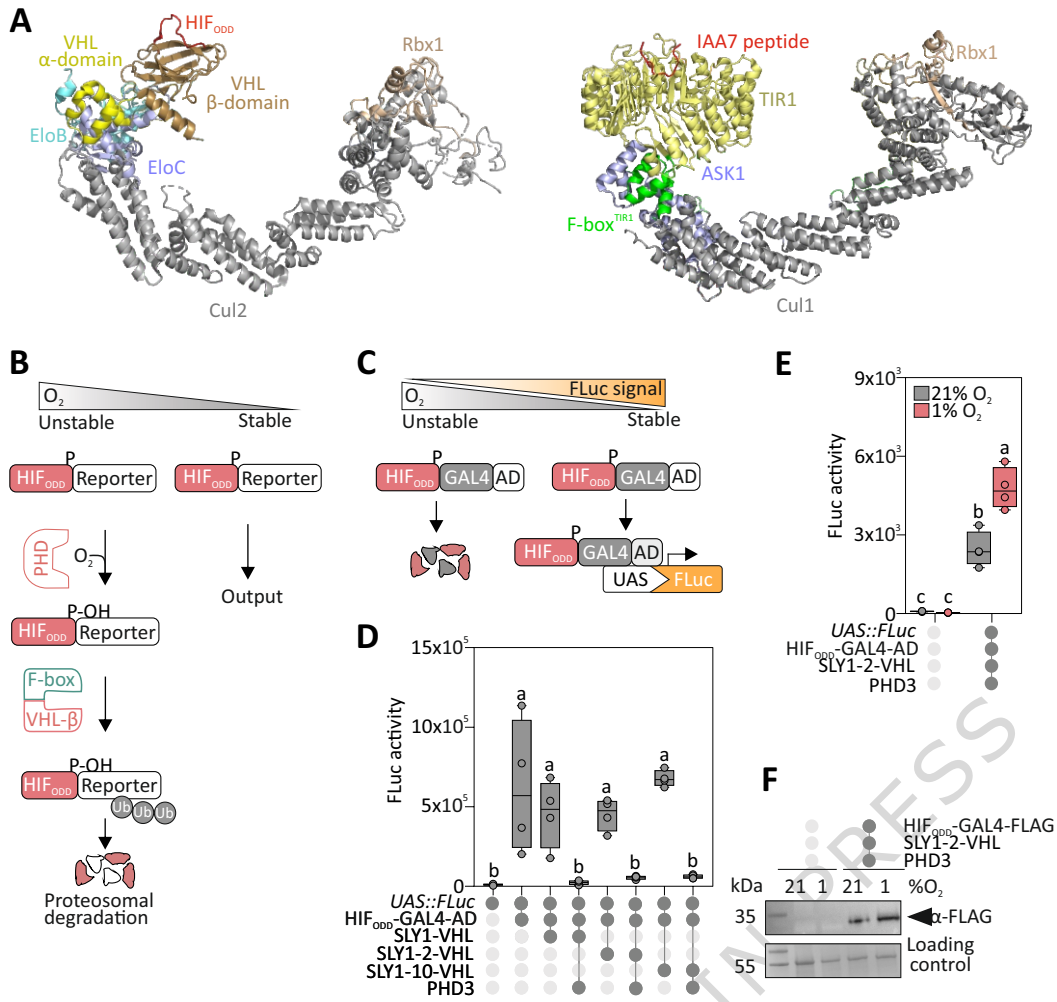
Figure 5. Synthetic control of petiole elongation under flooding-induced hypoxia. A. Design of a PIF4-HIF_{ODD} chimeric factor. Modifications applied to PIF4 to uncouple it from light, temperature and hormone regulation and rewire it to the mammalian-inspired synthetic O₂ sensing system devised in this study. **B.** Immunodetection of HIF_{ODD}-PIF4 in 7-day old seedlings following a treatment with 21% or 1% O₂ for 6 hours. Ponceau staining of total proteins is shown as the loading control. The Col-0 background is shown as a negative control. The experiment was repeated independently 2 times with similar results. **C.** Relative mRNA levels of HIF_{ODD}-PIF4 in 7-day old seedlings following a treatment with 21% or 1% O₂ for 6 hours. The Col-0 background is shown as a negative control. Data are mean \pm s.d. of $n = 3$ independent biological replicates, each consisting of RNA extracted from an independent pool of seedlings. **D.** Predicted regulation of HIF_{ODD}-PIF4. Under flooding-induced hypoxia, the HIF_{ODD}-PIF4 protein is stabilized, promoting petiole elongation. In normoxia and with active PHD3, HIF_{ODD}-PIF4 is targeted for degradation via SLY1-2-VHL. **E.** Phenotype of 2-week-old wild-type and PIF4-HIF_{ODD} plants treated for 4 days with darkness (control) or dark submergence. **F.** Quantification of petiole elongation from the plants in **(E)**. Letters indicate statistical significance, with two-way ANOVA and Tukey's post-test ($p \leq 0.05$). Data are mean individual petiole length of leaf number 4, per genotype and treatment, measured from independent plants. Data are shown as box plots, where the centre line indicates the median, box bounds indicate the 25th and 75th percentiles, whiskers extend to the minimum and maximum values, and all points represent individual biological replicates.

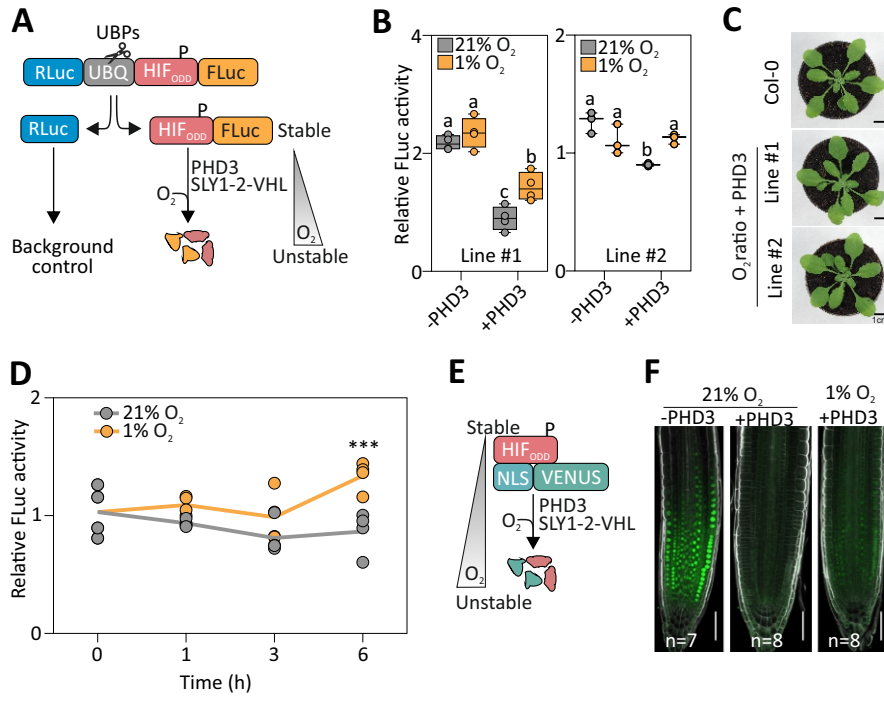
Editor's Summary:

A mammal-inspired synthetic oxygen sensor drives hypoxia responsive transcription in plants, replaces the native system in Arabidopsis, and regulates growth under flooding, offering new strategies to boost crop resilience.

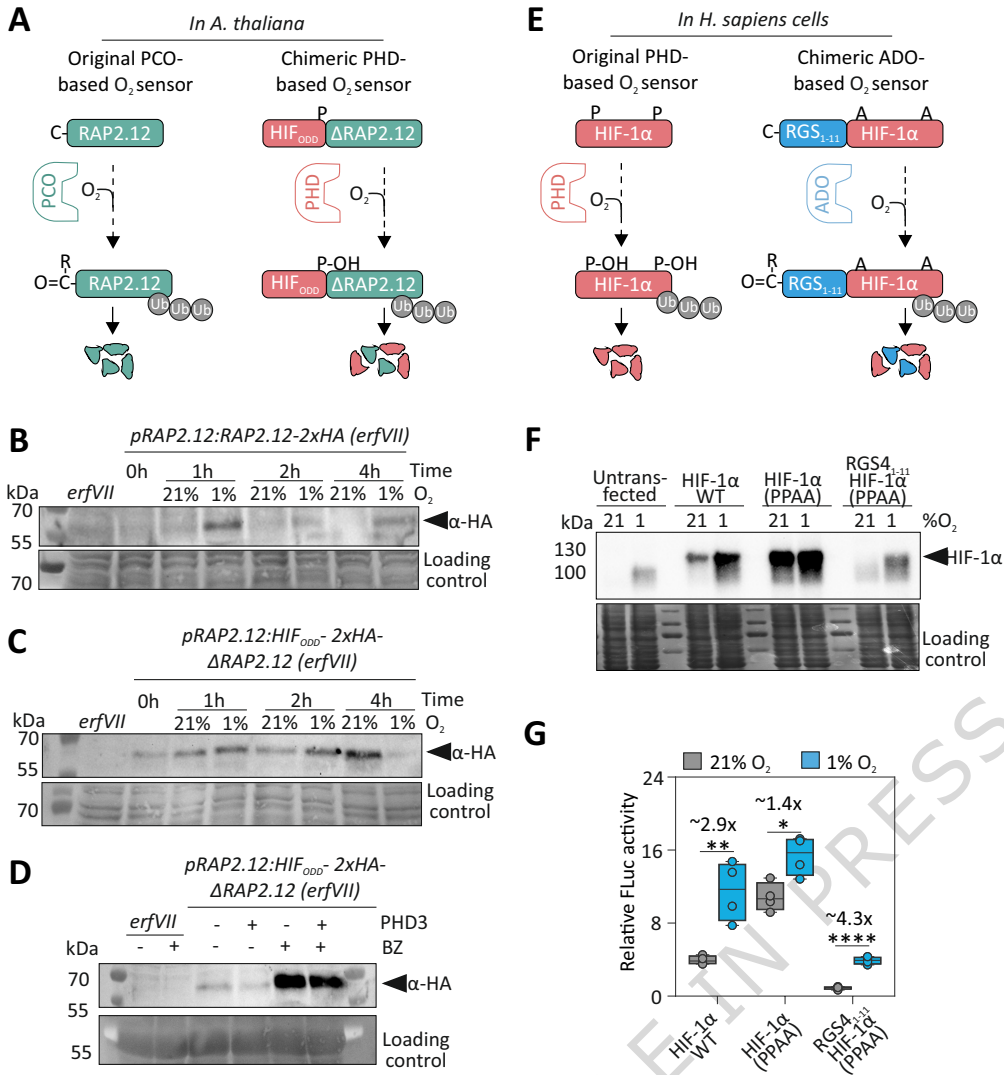
Peer review information: *Nature Communications* thanks Zhixing Cao who co-reviewed with Yiling Wang; Daniel Gibbs and the other anonymous reviewer(s) for their contribution to the peer review of this work. A peer review file is available.

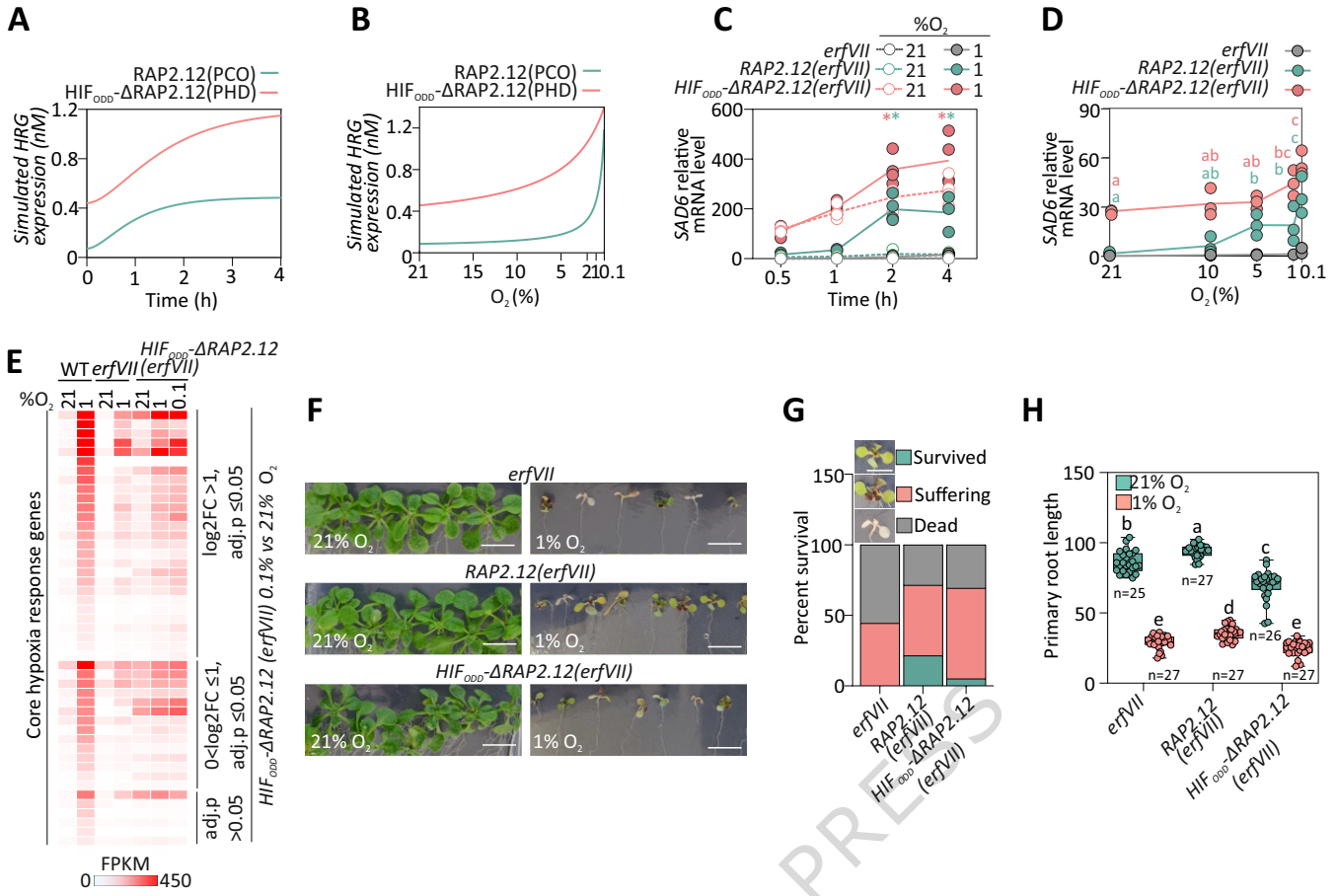
ARTICLE IN PRESS



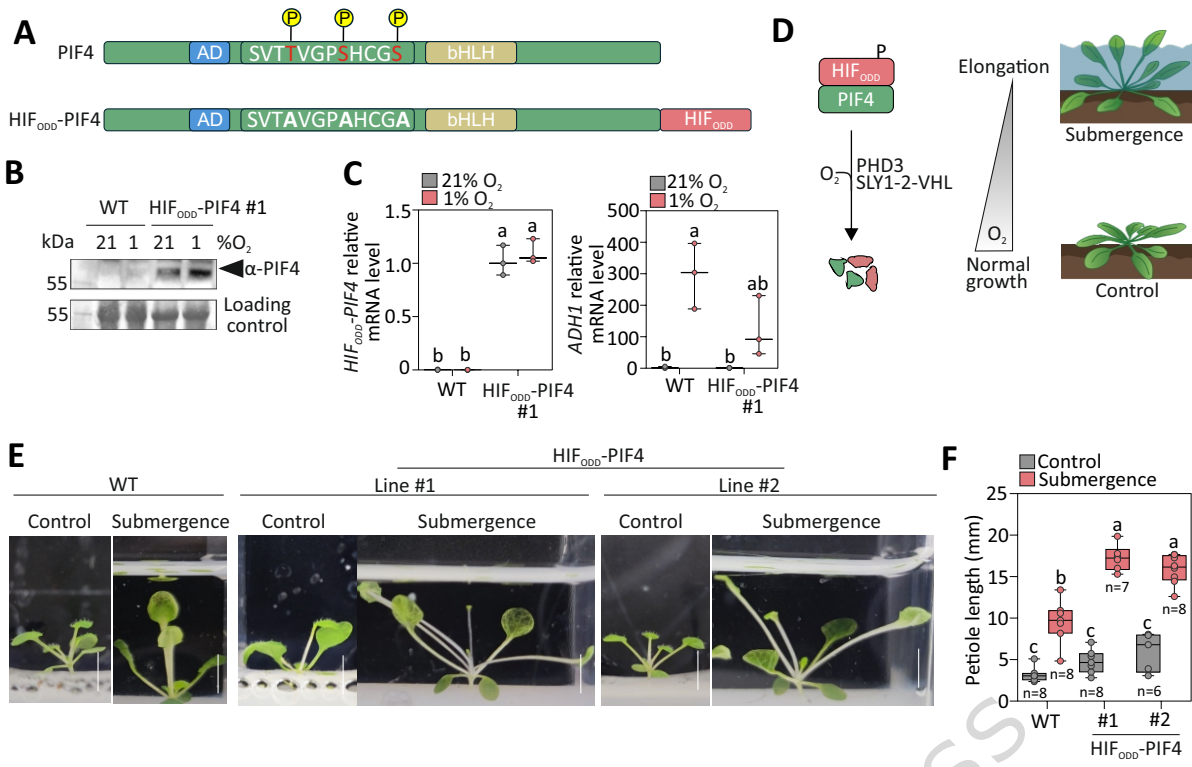


ARTICLE IN PRESS





ARTICLE IN PRESS



ARTICLE IN PRESS